Die approbierte gedruckte Originalversion dieser Diplomarbeit ist an der TU Wien Bibliothek verfügbar.
The approved original version of this thesis is available in print at TU Wien Bibliothek.

TECHNISCHE UNIVERSITÄT WIEN
Vienna University of Technology

Diplomarbeit

Combustion of Hydrocarbon Fuels and Liquid Alternative Fuels

Ausgführt zum Zwecke der Erlanungung des akademischen Grades eines Diplom-Ingenieurs unter der Leitung von

Ao.Univ.Prof.Dipl.-Ing. Dr.techn. Ernst Pucher
E 315 – Institut für Fahrzeugantriebe und Automobiltechnik
Technische Universität Wien

Prof. Dr. Kalyanasundaram Seshadri
Department of Mechanical and Aerospace Engineering
University of California, San Diego, USA

Eingereicht an der Technischen Universität Wien
Fakultät für Maschinenwesen und Betriebswissenschaften

von

Emanuel Höckner
Matrikel Nr.: 1028178
Baching 12
A-4926 St. Marienkirchen am Hausruck

TU Bibliothek Your knowledge hub WIEN

Combustion of Hydrocarbon Fuels and Liquid Alternative Fuels

Diploma Thesis

Emanuel Höckner

Institute of Internal Combustion Engines and Automotive Engineering

Vienna University of Technology

Advisor:

Ao. Univ-Prof. Dipl.-Ing. Dr.techn. Ernst Pucher
Institute of Powertrains and Automotive Technology
Vienna University of Technology, Austria

Prof. Dr. Kalyanasundaram Seshadri
Department of Mechanical and Aerospace Engineering
University of California, San Diego, US

Die approbierte gedruckte Originalversion dieser Diplomarbeit ist an der TU Wien Bibliothek verfügbar.
The approved original version of this thesis is available in print at TU Wien Bibliothek.

Abstract

Experimental investigations are carried out to elucidate the influences of the amount of fuel and oxygen on critical conditions of autoignition and extinction with the gaseous counterflow burner for propane and the liquid pool counterflow burner for n-heptane, isobutanol, n-heptane/isobutanol-mix, 1-propanol, ethanol, n-decane, n-decane/isobutanol-mix and butane in laminar non-premixed flows. The conditions of these fuels depend on the characteristic flow time and the characteristic chemical time. The characteristic flow time is given by the strain rate. The chemical time depends on the adiabatic flame temperature and the stoichiometric mixture fraction. The experiments are carried out employing the counterflow configuration. In the configuration of the gaseous counterflow burner, two streams flow toward a stagnation plane. One stream, called the fuel-stream, is made up of fuel and nitrogen, and the other stream, called the oxidizer-stream, is made up of oxygen and nitrogen. In the configuration of the counterflow liquid pool burner is also an oxidizer stream made up of oxygen and nitrogen but instead of the fuel stream is a cup filled with liquid fuel. The experiments were conducted at a pressure of 1.13 atm. The parameters that influence the autoignition and extinction experiments are the fuel mass fraction $Y_{F,1}$, the temperature of the fuel stream T_1, the oxygen mass fraction $Y_{O2,2}$, the temperature of the oxidizer stream T_2, and the strain rate a_2. The experiments were performed at the University of California in San Diego.

For the gaseous counterflow burner, critical conditions of extinction were measured at fixed values of the fuel mass fraction $Y_{F,1} = 0.6$, temperature of the fuel stream $T_1 = 295.15\ [K]$ and the temperature of the oxidizer stream $T_2 = 295.15\ [K]$. The strain rate at extinction aq, was measured for various values of the oxygen mass fraction $Y_{O2,2}$. Critical conditions of autoignition for the gaseous counterflow burner were measured at fixed values of the temperature of the fuel stream $T_1 = 294.15\ [K]$ and the strain rate $a = 400\ s^{-1}$. Two sets of experiments were performed with the gaseous counterflow-autoignition setup; in one set the oxygen mass fraction was fixed at $Y_{O2,2} = 0.23$ and the temperature of the oxidizer stream T_2 was measured for various values of the fuel mass fraction $Y_{F,1}$ and in the other set of experiments the fuel mass fraction was fixed at $Y_{F,1} = 0.21$ and the temperature of the oxidizer stream T_2 was measured for various values of the oxygen mass fraction $Y_{O2,2}$. For the liquid pool counterflow burner critical conditions of autoignition were measured at a fixed value of the oxygen mass fraction $Y_{O2,2} = 0.23$ and the temperature of the oxidizer stream T_2 was measured for various values of the strain rate a.

Die approbierte gedruckte Originalversion dieser Diplomarbeit ist an der TU Wien Bibliothek verfügbar.
The approved original version of this thesis is available in print at TU Wien Bibliothek.

Kurzfassung

Es werden Experimente durchgeführt um die Einflüsse der Brennstoff- und Sauerstoffmenge unter kritischen Bedingungen bei Selbstentzündung und Auslöschung von gasförmigen und flüssigen Kraftstoffen zu messen. In laminaren, nicht vorgemischten Strömungen wird mit einem Gegenstrombrenner für gasförmige Brennstoffe Propan getestet und mit einem Gegenstrombrenner für flüssige Brennstoffe werden n-Heptan, Isobutanol, ein n-Heptan/Isobutanol-Gemisch, 1-Propanol, Ethanol, n-Decan, ein n-Decan/Isobutanol-Gemisch und Butan untersucht. Die Eigenschaften dieser Brennstoffe hängen von der charakteristischen Auslaufzeit und von der charakteristischen chemischen Reaktionsdauer ab. Die charakteristische Auslaufzeit hängt wiederum von der Strain-Rate ab und die chemische Reaktionszeit steht in Abhängigkeit zur adiabaten Flammentemperatur und zur stöchiometrischen Mischungsfraktion. Die Experimente werden mit verschiedenen Konfigurationen eines Gegenstrombrenners durchgeführt. Bei dem Gegenstrombrenner für gasförmige Brennstoffe fließen zwei Strömungen zu einer Stagnations-Ebene zusammen. Die erste dieser beiden Strömungen wird als Brennstoffstrom bezeichnet und setzt sich aus dem jeweilig getesteten Kraftstoff und Stickstoff zusammen und die zweite Strömung wird als Oxidationsmittel-Strom bezeichnet und setzt sich aus Sauerstoff und Stickstoff zusammen. In dem Gegenstrombrenner für flüssige Brennstoffe befindet sich auch ein Oxidationsmittel-Strom aus Sauerstoff und Stickstoff aber anstatt eines Brennstoff-Stromes wird hier eine Tasse verwendet, die mit flüssigem Brennstoff befüllt wird. Die Versuche wurden bei einem Druck von 1.13 atm durchgeführt. Die Parameter die einen Einfluss auf die Selbstentzündungs- und Auslöschungsexperimente haben sind der Brennstoff-Massenanteil $Y_{F,1}$, die Temperatur des Brennstoffstromes T_1, der Sauerstoff-Massenanteil $Y_{O2,2}$, die Temperatur des Oxidationsmittel-Stromes T_2 und die Strain-Rate a_2. Die Experimente wurden an der University of California in San Diego durchgeführt.

Beim Auslöschungs-Experiment für gasförmige Brennstoffe wurde der Brennstoff-Massenanteil auf $Y_{F,1} = 0.6$, die Temperatur des Brennstoff-Stromes auf $T_1 = 295.15\ [K]$ und die Temperatur des Oxidationsmittel-Stromes auf $T_2 = 295.15\ [K]$ fixiert und der Sauerstoffmassen-Anteil $Y_{O2,2}$ variiert um für den jeweiligen Wert die Strain-Rate zu messen. Beim Selbstentzündungs-Experiment für gasförmige Brennstoffe wurde die Temperatur des Brennstoff-Massenanteil auf $T_1 = 294.15\ [K]$ und die Strain-Rate auf $a = 400s^{-1}$ fixiert um zwei verschiedene Versuchsreihen durchzuführen. In der ersten Versuchsreihe wurde zusätzlich der Sauerstoff-Massenanteil auf $Y_{O2,2} = 0.23$ fixiert und der Brennstoff-Massenanteil $Y_{F,1}$ über mehrere Werte variiert um für den jeweiligen Wert die Temperatur des Oxidationsmittel-Stromes T_2 zu messen. In der zweite Versuchsreihe wurde der

Die approbierte gedruckte Originalversion dieser Diplomarbeit ist an der TU Wien Bibliothek verfügbar.
The approved original version of this thesis is available in print at TU Wien Bibliothek.
TU Bibliothek Your knowledge hub WIEN

Brennstoff-Massenstrom auf $Y_{F,1} = 0.21$ fixiert und der Sauerstoff-Massenstrom über mehrere Werte variiert um für den jeweiligen Wert die Temperatur des Oxidationsmittel-Stromes T_2 zu messen. Beim Auslöschungs-Experiment für gasförmige Brennstoffe wurde der Sauerstoffmassen-Anteil auf $Y_{O2,2} = 0.23$ und die Temperatur des Brennstoff-Stromes auf $T_1 = 294.15\ [K]$ fixiert und die Strain-Rate a_2 über mehrere Werte variiert um für den jeweiligen Wert die Temperatur des Oxidationsmittel-Stromes T_2 zu messen.

Die approbierte gedruckte Originalversion dieser Diplomarbeit ist an der TU Wien Bibliothek verfügbar.
The approved original version of this thesis is available in print at TU Wien Bibliothek.

Acknowledgements

Throughout the writing of this thesis I have received a great deal of support and assistance.

First and foremost I would like to express my sincere gratitude to Professor Ernst Pucher from the Institute for Powertrains and Automotive Technology of the Technical University of Vienna who offered me this opportunity to write my master-thesis at the University of California in San Diego. Without his guidance and support I would have never been able to work with the best in the field of combustion science at the UCSD.

Furthermore I would like to thank Professor Kalyanasundaram Seshadri from the Institute of Mechanical Engineering of the University of California in San Diego for his patience, encouragement and immense knowledge. The door to Professor Seshadri was always open whenever I ran into a trouble spot or had a question about my research or writing of this thesis.

My sincere thanks also go to my research co-worker Martin Hunyadi-Gall. He was not only a great advisor in the lab but also the best guide I could wish for related to everything personal during my time in California. Thank you for that.

Last but definitely not least I want to express my profound gratitude to my family, especially my parents, my two brothers and my sister. They always provided me with unfailing support through my years of study and my time I spent abroad for this thesis. This journey would not have been possible if not for them, and I dedicate this milestone to them.

Die approbierte gedruckte Originalversion dieser Diplomarbeit ist an der TU Wien Bibliothek verfügbar.
The approved original version of this thesis is available in print at TU Wien Bibliothek.

Table of content

List of Symbols VII
Subscripts IX
Nomenclature X
1. Introduction 1
2. Fundamentals in Combustion Physics and Chemical Kinetics of Hydrocarbons and Alcohol 2
2.1 Thermodynamics and Chemical Kinetics 2
2.1.1 The Laws of Thermodynamics 2
2.1.2 Thermodynamic Functions 3
2.1.3 Branched-chain explosions 5
2.2 Mechanisms of Hydrocarbon and Alcohols 7
2.2.1 The Oxidation of Higher-Order Hydrocarbons 7
2.2.2 The Oxidation of Alcohols 8
2.3 Laminar Diffusion Flames 10
2.3.1 The Planar Counterflow Diffusion Flame 10
2.3.2 Steady State Combustion and Quenching of Diffusion Flames with One-Step Chemistry 11
3. Apparatus and Procedure 13
3.1 Tested Fuels 14
3.1.1 Hydrocarbons 14
3.1.2 Alcohols 15
3.2 Counterflow Burner 17
3.2.1 Lower Part of the Counterflow Burner 17
3.2.2 Upper Part of the Counterflow Burner 18
3.2.2.1 Extinction Top 18
3.2.2.2 Autoignition Top 20
3.3 Liquid Pool Burner 21
3.3.1 Lower Part of the Liquid Pool Burner 21
3.3.2 Upper Part of the Liquid Pool Burner 22
3.4 LabView Controlling Software 22
3.5 Gas Flow Control and Calibration 23
3.6 Temperature Measurement and Control 24
3.6.1 Temperature Correction 25
3.7 Experimental Procedures 27
3.7.1 Experimental Procedures of the Gaseous Counterflow Burner ... 27
3.7.2 Experimental Procedures of the Liquid Pool Counterflow Burner 29
4. Discussion of the Experimental Results of the Atmospheric Pressure Counterflow Burner 31

Die approbierte gedruckte Originalversion dieser Diplomarbeit ist an der TU Wien Bibliothek verfügbar.
The approved original version of this thesis is available in print at TU Wien Bibliothek.
TU Bibliothek Your knowledge hub WIEN

4.1 Discussion of the Experimental Results of the Gaseous Counterflow Burner 31
4.1.1 Results of the Autoignition Experiments 31
4.1.2 Results of the Extinction Experiments 34
4.2 Discussion of the Experimental Results of the Liquid Pool Counterflow Burner 35
4.2.1 Results of the Autoignition Experiments 35
5. Concluding Remarks 47

Die approbierte gedruckte Originalversion dieser Diplomarbeit ist an der TU Wien Bibliothek verfügbar.
The approved original version of this thesis is available in print at TU Wien Bibliothek.
TU Bibliothek Your knowledge hub WIEN

List of Symbols

A	Helmholtz free energy [J]
a	Strain rate [1/s]
c	General heat/thermal capacity [J K^{-1}]
cp	Heat capacity [kJ/kgK]
D_a	Damköhler number [-]
d	Thermocouple diameter [mm]
E	Activation Energy [J/mol]
G	Gibbs free energy [J]
H	Enthalpy [J]
h	Heat transfer rate coefficient [-]
k	Thermal conductivity [W/mK]
k	Rate constant [-]
N	Number of molecules [-]
n	Number of moles [mol]
Nu	Nusselt number [-]
p	Pressure [Pa]
Q	Heat Energy [J]
R	Gas constant [J/molK]
Re	Reynolds number [-]
S	Entropie [J K^{-1}]
T	Temperature [K]
U	Internal Energy [J]
u	nondimensional function related to radial component of velocity
V	Volume [m^3]
v	kinemativ viscocity
v	nondimensional axial component of velocity
W	work [J]
x	velocity component in x-direction [m/s]
Y	Mass fraction [-]
y	velocity component in y-direction [m/s]
Z	Partition function [-]
z	velocity component in z-direction [m/s]
α	Branching constant [-]

Die approbierte gedruckte Originalversion dieser Diplomarbeit ist an der TU Wien Bibliothek verfügbar.
The approved original version of this thesis is available in print at TU Wien Bibliothek.
TU Bibliothek Your knowledge hub WIEN

β	Number of termination steps [-]
δ	Extinction condition [-]
ε	Emissivity [-]
μ	Chemical potential [J]
ρ	Density [kg/m^3]
σ	Stefan –Boltzmann constant [W/m^{2}K^4]
χ	Dissipation rate [m^2/s^3]
ω	Landau Potential [J]

Die approbierte gedruckte Originalversion dieser Diplomarbeit ist an der TU Wien Bibliothek verfügbar.
The approved original version of this thesis is available in print at TU Wien Bibliothek.

Subscripts

1	Fuel side
2	Oxidizer side
cat	surface-induced catalytic reactions
cond	Conduction
conv	Convection
rad	Radiation
q	Quenching
st	steady state
surr	Surroundings
tc	Thermocouple

Die approbierte gedruckte Originalversion dieser Diplomarbeit ist an der TU Wien Bibliothek verfügbar.
The approved original version of this thesis is available in print at TU Wien Bibliothek.

Nomenclature

CO	Carbon monoxide
CO_2	Carbon dioxide
H_2O	Water
H	Hydrogen
O	Oxygen
OH	Hydroxide

Die approbierte gedruckte Originalversion dieser Diplomarbeit ist an der TU Wien Bibliothek verfügbar.
The approved original version of this thesis is available in print at TU Wien Bibliothek.

1. Introduction

Alternative fuels like biofuels have been around as long as the automobile exists. Henry Ford for example planned to fuel his Model Ts with ethanol at the start of the 20th century and early diesel engines were shown to run on peanut oil. But discoveries of huge petroleum deposits kept gasoline and diesel cheap for decades, and those alternative fuels were largely forgotten. However, with the recent rise in oil prices, along with growing concern about global warming caused by carbon dioxide emissions, alternative fuels have been regaining popularity. Countries around the world are using various kinds of biofuels. For decades, Brazil has turned sugarcane into ethanol, and some cars there can run on pure ethanol rather than as additive to fossil fuels. And biodiesel—a diesel-like fuel commonly made from palm oil—is generally available in Europe. On the face of it, those examples of alternative fuels look like a great solution because cars are a major source of atmospheric carbon dioxide, the main greenhouse gas that causes global warming. But since plants absorb carbon dioxide as they grow, crops grown for biofuels should suck up about as much carbon dioxide as comes out of the tailpipes of cars that burn these fuels. Unfortunately the process of growing the crops, making fertilizers and pesticides, and processing the plants into fuel consumes a lot of energy and much of the energy used in production comes from coal and natural gas. So it is very important to not only use alternative fuels instead of conventional ones like gasoline and diesel in order to reduce emissions, but also to use as much renewable energy as possible in the process of producing alternative fuels.

But despite the growing interest in alternatives to gasoline and diesel powered engines it is apparent that these conventional combustion engines will continue to dominate as a drive concept in vehicles over the next few decades due to their flexibility, compactness and efficiency. For this purpose it is necessary to, not only understand the fundamental processes during the combustion of alternative fuels but also during the combustion of conventional fuels to reduce the resulting pollutants in order to allow the cleanest possible road traffic and to reduce emissions in general.

The research described here is concerned with fundamental mechanisms of autoignition and extinction of hydrocarbons and alternative fuels studied by employing a counter flow configuration for gaseous fuels as well as a counterflow configuration for liquid fuels. The thesis involves a theoretical part on fundamentals in combustion physics and chemical kinetics of hydrocarbons and alcohols as well as an experimental section on structures of hydrocarbon and alcohol diffusion flames, carried out with the gaseous counterflow burner for propane and the liquid pool counterflow burner for n-heptane, isobutanol, n-

Die approbierte gedruckte Originalversion dieser Diplomarbeit ist an der TU Wien Bibliothek verfügbar.
The approved original version of this thesis is available in print at TU Wien Bibliothek.
TU Bibliothek Your knowledge hub WIEN

heptane/isobutanol-mix, 1-propanol, ethanol, n-decane, n-decane/isobutanol-mix and butane.

2. Fundamentals in Combustion Physics and Chemical Kinetics of Hydrocarbons and Alcohol

2.1 Thermodynamics and Chemical Kinetics

2.1.1 The Laws of Thermodynamics

For specifying the thermodynamic state of the system, the quantities p, V, N_i $(i = 1, ..., N)$ constitute a convenient complete set of independent variables in an open chemical system. The volume V and the mole number N_i $(i = 1, ..., N)$ are extensive variables, while the pressure p is an intensive property. The numbers of moles of the same species present in different phases are distinguished by different values of the subscript i, so that N is the *sum* of the total number of species present in each phase.

Temperature T = $T(p, V, N_i)$, which has the same value for all systems in equilibrium with each other, is an additional intensive variable which is stated by the zeroth law of thermodynamics. There is an extensive function $U = U(p, V, N,)$, called the internal energy, stated by the first law of thermodynamics which describes the conservation of energy. Having the property for a closed system, one that does not exchange material with its surroundings, the heat added to the system in an infinitesimal process is

$$dQ = dU + p\,dV \tag{2.1}$$

There exists an absolute scale for the temperature T and an extensive function $S(p, V, N_i)$ which is called the entropy, stated by the classical formulation of the second law of thermodynamics. Such that for an infinitesimal process in a closed system

$$T\,dS \geq dQ \tag{2.2}$$

where the inequality is valid for natural processes and the equality holds for reversible processes. The third law of thermodynamics appears to be of little use in combustion because of the particular results of statistical mechanics. [1]

Die approbierte gedruckte Originalversion dieser Diplomarbeit ist an der TU Wien Bibliothek verfügbar.
The approved original version of this thesis is available in print at TU Wien Bibliothek.

2.1.2 Thermodynamic Functions

From equations (2.1) and (2.2) it follows that $T = (U/S)_{V, Ni}$ and $p = -(U/V)_{S, Ni}$, whence by defining the chemical potential of a given species in a given phase as [1]

$$\mu_i \equiv (\partial U/\partial N_i)_{S, V, Nj(j\neq i)} \tag{2.3}$$

It is found that

$$dU = T\,dS - p\,dV + \sum_{i=1}^{N} \mu i\, dN_i\,. \tag{2.4}$$

It is seen that the Helmholtz function $A \equiv U - TS$ from equation (2.4), the Gibbs function $G \equiv H - TS$ and the enthalpy $H \equiv U + pV$ obey the relations [2]

$$dA = -S\,dT - p\,dV + \sum_{i=1}^{N} \mu i\, dN_i \tag{2.5}$$

$$dH = T\,dS + V\,dp + \sum_{i=1}^{N} \mu i\, dN_i \tag{2.6}$$

and

$$dG = -S\,dT + V\,dp + \sum_{i=1}^{N} \mu i\, dN_i \tag{2.7}$$

Equation (2.7) shows that μ_i is the partial molar Gibbs function, since the partial molar value (with respect to i) of any extensive property is defined as $\chi\ (\chi/N_i)_{p, T, Nj(ji)}$.

Equation (2.4) - (2.7) are very useful in providing general relations between thermodynamic properties. They display a certain degree of symmetry and have been called the *fundamental equations* of chemical thermodynamics. [3] It follows from equation (2.7) for example that

$$(\partial S/\partial p)_{T, Ni} = -(\partial V/\partial T)_{p, Ni} \tag{2.8}$$

This type of relation is usually called *Maxwell* equations. Furthermore, if any one of the properties *U, A, H,* or *G* is known as a function of the independent variables appearing in its fundamental equation, then all the other thermodynamic properties can be evaluated as functions of these independent variables by using the

Die approbierte gedruckte Originalversion dieser Diplomarbeit ist an der TU Wien Bibliothek verfügbar.
The approved original version of this thesis is available in print at TU Wien Bibliothek.
TU Bibliothek Your knowledge hub WIEN

appropriate fundamental equation and property definitions to relate the unknown properties to the known function and its derivatives. [1] By using the fact that *G* is an extensive property, an integrated relation of completely general validity between *G* and the μ_i 's and N_i 's can be obtained from equation (6). All intensive properties remain constant and all extensive properties increase proportionally in a "process" in which the size of the system is increased by adding systems with the same intensive properties. Equation (2.7) shows it can be readily integrated hence $dT = 0$, $dp = 0$, and $d\mu_i = 0$ from $G = 0$, $N_i = 0$ to G, N_i, yielding

$$G = \sum_{i=1}^{N} \mu i \, Ni. \qquad (2.9)$$

For the counterflow and liquid pool experiments it is very important to show the equilibrium of the system. This equilibrium can always be found at the minimum of G in the correlation between G and T. So therefore the equation in (2.9) can be used to find the minimum of G, respectively the equilibrium of the counterflow burning system.

The results of similar integrations performed in equations (2.4) – (2.6) are always equivalent to equation (2.9), without obtaining new relationships. On the other hand, the same procedure may be used in conjunction with the general relation

$$d\chi = \left(\frac{\partial \chi}{\partial T}\right)_{p,\, Ni} dT + \left(\frac{\partial \chi}{\partial p}\right)_{T,\, Ni} dp + \sum_{i=1}^{N} \left(\frac{\partial \chi}{\partial Ni}\right)_{p,\, T,\, Nj\,(j \neq i)} dN_i \qquad (2.10)$$

to show that any extensive property χ may be expressed in terms of its partial molar values, namely

$$\chi = \sum_{i=1}^{N} \left(\frac{\partial \chi}{\partial Ni}\right)_{p,\, T,\, Nj\,(j \neq i)} N_i \qquad (2.11)$$

Substituting the result into equation (2.7) and differentiating equation (2.9) gives

$$\sum_{i=1}^{N} Ni \; d\mu i = -S \, dT + V \, dp \qquad (2.12)$$

a general result which is useful in discussions of phase equilibria for the counterflow combustion systems. [1]

Die approbierte gedruckte Originalversion dieser Diplomarbeit ist an der TU Wien Bibliothek verfügbar.
The approved original version of this thesis is available in print at TU Wien Bibliothek.

2.1.3 Branched-chain explosions

There are two different ways in which explosions in approximately homogeneous chemical systems, like in combustions with counterflow burner systems, have been studied experimentally. The first being by introducing reactants into a preheated vessel by the use of a piston-driven adiabatic compression to achieve a rapid increase in temperature and the second being by shock-tube techniques in which a shock wave produces compression. The temperature increase in these experiments initiates measurable rates of reaction and those reaction histories are recorded with the objective of ascertaining whether the heat-release rate eventually experiences an abrupt increase. This kind of heat release would be classified as an explosion and the time that elapses before this increase occurs would also be recorded. To illustrate how chain branching may be responsible for such explosions, a simplified kinetic model may be employed where R signifies a reactant, P signifies a product, and C signifies the chain carrier. The initiation, propagation and termination steps are written as $R \rightarrow C$, $C + R \rightarrow P + \alpha C$ and $C \rightarrow P$, where α is a branching constant, equal to unity for straight-chain reactions. Following equation

$$dc_i/dt = \omega_i , \qquad i = 1, \dots , N. \tag{2.13}$$

with k_i, k_p and k_t representing the rate constants for these three steps, equation (2.13) gives

$$dc_R/dt = -k_i\, cR - k_p\, c_R\, c_C , \qquad dcp/dt = k_p\, c_R\, c_R\, c_C + k_t\, c_C, \tag{2.14}$$

and

$$dc_C/dt = k_i\, c_R + (\alpha - 1)\, k_p\, c_R\, c_C - k_t\, c_C \tag{2.15}$$

It has been seen that dc_C/dt decreases with t if $k_t > (\alpha - 1)\, K_p\, C_R(0)$, in k_i (less strongly), or in k_t (much less strongly) produces a decrease of the induction time. There are elements of arbitrariness in the definition of induction time as well as in judgments of whether explosion occurs. [1]

Die approbierte gedruckte Originalversion dieser Diplomarbeit ist an der TU Wien Bibliothek verfügbar.
The approved original version of this thesis is available in print at TU Wien Bibliothek.

Since it has been seen that dcC/dt decreases with t if $kt > (\alpha - 1)\, kp\, cR(0)$ but may exhibit an explosion-like growth if $kt < (\alpha - 1)\, kp\, cR(0)$, it may be reasonable to identify the equality $kt = (\alpha - 1)\, kp\, cR(0)$ with the boundary of explosion. [1] The steady-state approximation for the intermediary C is making use of the alternative reasoning that leads to this same result. Vanishing of the right-hand side of equation (2.15) yields

$$c_C = (ki/kp)/[\beta - (\alpha - 1)] \tag{2.16}$$

where $\beta = kt/(kp\, cR)$ measures the number of the termination steps per propagation step experienced by C. Substitution of equation (2.16) into equation (2.14) yields

$$dcp/dt = ki(cR + kt/kp)/[\beta - (\alpha - 1)] \tag{2.17}$$

for the overall rate of production of products. The steady-state approximation may be acceptable if $\beta > \alpha - 1$, then equations (2.16) and (2.17) provide positive values for c_C. The steady state is clearly not acceptable under this condition if $\beta \leq \alpha - 1$, then equation (2.16) yields an infinite or negative value of c_C. The limit in which the steady state predicts the infinite c_C and rate has been identified as the explosion limit and agrees with the estimate obtained above. [1] Hence,

$$\alpha \geq 1 + \beta \tag{2.18}$$

may be employed as a criterion for the occurance of a branched-chain explosion. Phenomenological reasoning and approximate analyses of different simplified models for the reacting system are including alternative approaches to derivations that lead to results such as those given in equations (2.17) and (2.18). [4] [5] [6]

Die approbierte gedruckte Originalversion dieser Diplomarbeit ist an der TU Wien Bibliothek verfügbar.
The approved original version of this thesis is available in print at TU Wien Bibliothek.

2.2 Mechanisms of Hydrocarbons and Alcohols

2.2.1 The Oxidation of Higher-Order Hydrocarbons

The greater instability of the higher-order alkyl radicals and the great variety of minor species that can form (see Table 1) makes the high-temperature oxidation of paraffins larger than methane a fairly complicated subject. But despite these complications, there are detailed models of methane [7 – 9], ethane [10], propane [11] and many other hydrocarbons [12] available in the literature, so it is possible to develop a general framework of important steps that elucidates this complex subject.

Fuel	Relative Hydrocarbon Intermediate Concentrations
Ethane	Ethene $\geq$ methane
Propane	Ethene $>$ propene $\geq$ methane $>$ ethane
Butane	Ethene $>$ propene $\geq$ methane $>$ ethane
Hexane	Ethene $>$ propene $>$ butene $>$ methane $\geq$ pentene $>$ ethane
2-Methylpentane	Propene $>$ ethene $>$ butene $>$ methane $\geq$ pentene $>$ ethane

Table 1: Relative Importance of Intermediates in Hydrocarbon Combustion

As suggested very early by Fristrom and Westenberg [13], it is interesting to review a general pattern for oxidation of hydrocarbons in flames. The primary zone and the secondary zone are two essential thermal zones suggested by Fristrom and Westenberg. The primary zone describes the initial hydrocarbons, which are attacked and reduced to products (CO, H_2, H_2O) and radicals (H, O, OH), whereas the secondary zone is describing the complete oxidation of CO and H_2. The intermediates are said to form in the primary zone. Hydrocarbons of lower order than the initial fuel appear to form in oxygen-rich, saturated-hydrocarbon flames according to

$$\{OH + C_nH_{2n+2} \rightarrow H_2O + [C_nH_{2n+1}\} \rightarrow C_{n-1}H_{2n-2} + CH_3] \qquad (2.19)$$

The initial radical C_nH_{2n+1} usually splits off CH_3 and forms the next lower-order olefinic compound because hydrocarbon radicals of higher order than ethyl are unstable. There is fission into an olefinic compound and a lower-order radical with hydrocarbons of higher order than C_3H_8. O, H, and OH rapidly attack the

Die approbierte gedruckte Originalversion dieser Diplomarbeit ist an der TU Wien Bibliothek verfügbar.
The approved original version of this thesis is available in print at TU Wien Bibliothek.

formaldehyde that forms in the oxidation of the fuel and of the radicals so that formaldehyde is usually found only as a trace in flames.

The initial reaction is simply the H abstraction analogous to the preceding OH reaction, although Fristrom and Westenberg claimed that the situation is more complex in fuel-rich saturated-hydrocarbon flames. For example,

$$H + C_nH_{2n+2} \rightarrow H_2 + C_2H_{2n+1} \qquad (2.20)$$

Hydrocarbons of order higher than the original fuel are formed as intermediates and under these conditions the concentrations of H and other radicals are large enough that their recombination becomes important.

High-temperature flow-reactor studies confirmed the general features suggested by Fristrom and Westenberg, however this work permits more detailed understanding of the high-temperature oxidation mechanism and shows that under oxygen-rich conditions the initial attack by O atoms must be considered as well as the primary OH attack. [14] More importantly the fuel is consumed to a major extent, before significant energy release occurs and it has been established that the paraffin reactants produce intermediate products that are primarily olefinic. During the conversion of the fuel, the initial temperature increases with the amount of energy that is being released. This leads to the conclusion that the olefin oxidation rate simply increases more appreciably with temperature, and the olefins are being oxidized while they are being formed from the fuel.

2.2.2 The Oxidation of Alcohols

Alcohol combustion chemistry is an interesting variation of the analogous paraffin hydrocarbon, mainly because of the presence of the OH group in alcohols. Consequently, many of the C-H bond strengths are different than their values for structurally similar nonoxygenated hydrocarbons and the oxygen atom in the molecular structure generally alters the electronic structure. There are two different fundamental ways in the initial attack on alcohols. In one, the OH group can be displaced while an alkyl radical also remains as a product. In the other, the alcohol is attacked at a different site and forms an intermediate oxygenated species, typically an aldehyde. [14] The bond strengths in the particular alcohol molecule and the

Die approbierte gedruckte Originalversion dieser Diplomarbeit ist an der TU Wien Bibliothek verfügbar.
The approved original version of this thesis is available in print at TU Wien Bibliothek.

overall stoichiometry that determines the relative abundance of the reactive radicals are dependent on the dominant pathway.

The mechanism of ethanol oxidation has now been studied in flow and stirred reactors, shock tubes, and flames over a wide range of temperature and pressure. [14] Acetaldehyde and ethene are assumed to form directly from ethanol although in flow reactor studies [15] acetaldehyde appears earlier in the reaction than ethane does. No direct mechanisms for the formation of ethene from acetaldehyde are indicated by any studies of acetaldehyde oxidation [16].

Unlike methanol, ethanol does not lose the OH group in an initiation step because of the fact that C-C bonds are weaker than the C-OH bond. The radical pool, which is led by the dominant initial step, is

$$C_2H_5OH + M \rightarrow CH_3 + CH_2OH + M \qquad (2.21)$$

This initiation step does not appear to contribute significantly to the product distribution as in all long-chain fuel processes and, indeed, no formaldehyde is observed experimentally as a reaction intermediate. There is also indication in flames that H_2O elimination through a complex fission reaction involving a four-centered transition state can yield ethene directly [14]

$$C_2H_5OH + M \rightarrow C_2H_4 + H_2O + M \qquad (2.22)$$

Formations of three isomers of C_2H_5O are led by hydrogen abstraction. Due to the weakness of this bond strength (~397 kJ/mol) in the proximity of the electrophilic O atom, the favored reaction is abstraction of an H atom from the α C-H bond. The CH_3CHOH radical is then consumed by dissociation or reaction with O_2 as described in equation (2.23) and (2.24). [14]

$$C_2H_5OH + X \rightarrow CH_3CHOH + XH \qquad (2.23)$$

$$CH_3CHOH + \binom{M}{O_2} \rightarrow CH_3CHO + \binom{H+M}{HO_2} \qquad (2.24)$$

Die approbierte gedruckte Originalversion dieser Diplomarbeit ist an der TU Wien Bibliothek verfügbar.
The approved original version of this thesis is available in print at TU Wien Bibliothek.

Ethanol oxidation, just like methanol oxidation shows a variation in the relative concentration of intermediate species according to the overall stoichiometry. This is because the initial oxygen concentration determines the relative abundance of specific abstracting radicals.

2.3 Laminar Diffusion Flames

2.3.1 The Planar Counterflow Diffusion Flame

Counterflow diffusion flames are very often used experimentally because they represent an essentially one-dimension diffusion flame structure. [17] There are two typical cases where counterflow flames have been established between an oxidizer stream from above and a fuel stream from below, as shown in Figure 1. The fuel stream from below may be either a gaseous fuel or an evaporating liquid fuel. The flame is embedded between two potential flows, one coming from the oxidizer and one from the fuel side. This fact is under the assumption that the flow velocities of both streams are sufficiently large and sufficiently removed from the stagnation plane. The potential flow velocity gradient in the oxidizer stream can be depicted as $a = -\partial v_\infty/\partial y$. The velocities and the mixture fraction are

$$y \to \infty : \quad v_\infty = -ay, \; u_\infty = ax, \qquad Z = 0. \tag{2.25}$$

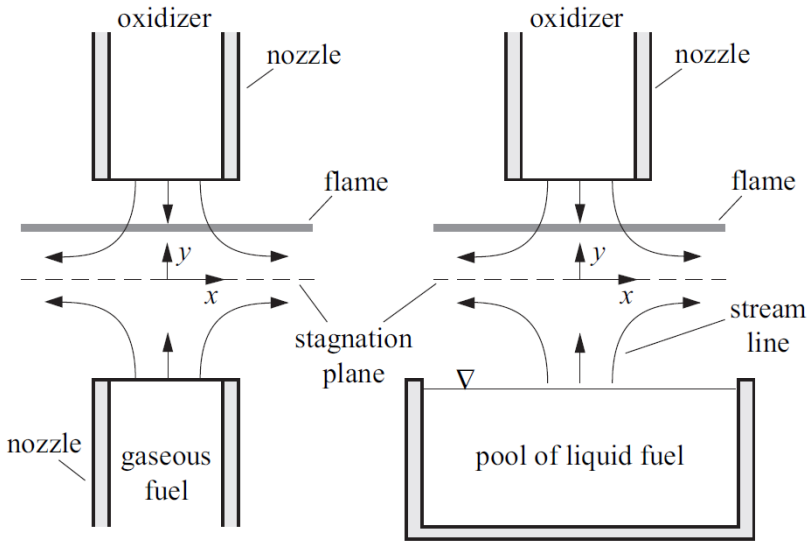

Figure 1: A schematic illustration of the experimental configuration for counterflow flames for gaseous and liquid fuels

Die approbierte gedruckte Originalversion dieser Diplomarbeit ist an der TU Wien Bibliothek verfügbar.
The approved original version of this thesis is available in print at TU Wien Bibliothek.

2.3.2 Steady State Combustion and Quenching of Diffusion Flames with One-Step Chemistry

Depending on different flow and boundary conditions, laminar counterflow diffusion flames have in general two different burning limits. These two different burning limits are called the point of extinction and the point of autoignition. The relevant information, which can be gained from a steady-state viewpoint, is whether the system is ignitable or extinguishable, instead of analyzing the extinction and the transient ignition processes [18]. The maximum reaction temperature in the reactive flow-field or the burning rates as a function of a corresponding system Damköhler number are plotted to visualize these two combustion limits [19] [20]. All the possible steady chemical states that a given reacting mixture can achieve are illustrated with the commonly known S-shaped curve (as shown in Figure 2), which is characterized by two stable branches and by one unstable branch. The lower reacting flow branch of the S-curve, where the reaction rates are insignificant, represents the chemically frozen flow limit. By increasing the Damköhler number and by decreasing the strain rate, the chemical rate increases along the lower branch. The residence time of the reactants in the mixing layer is extended when the strain rate is decreased. This leads to higher rates of reactants in the mixing layer, which then results into the ignition event occurring at D_a = Daign, where the heat loss in a steady state is exceeded by the heat generation. An increase in strain rate and a decreasing D_a leads to a lower residence time of the reactants in the mixing layer and also to a decrease in temperature, in contrast to a reduction in the strain rate. The flame is unable to sustain steady burning and extinguishes because not all of the chemical energy can be released during the finite residence time in the reaction layer. [21] [18]

Die approbierte gedruckte Originalversion dieser Diplomarbeit ist an der TU Wien Bibliothek verfügbar.
The approved original version of this thesis is available in print at TU Wien Bibliothek.
TU Bibliothek Your knowledge hub WIEN

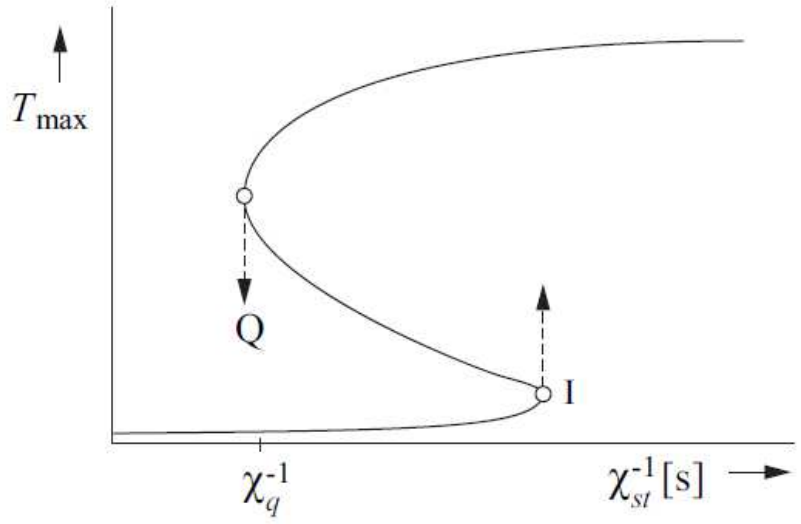

Figure 2: The S-shaped curve showing the maximum temperature in a diffusion flame as a function of the inverse of the scalar dissipation rate at stoichiometric mixture

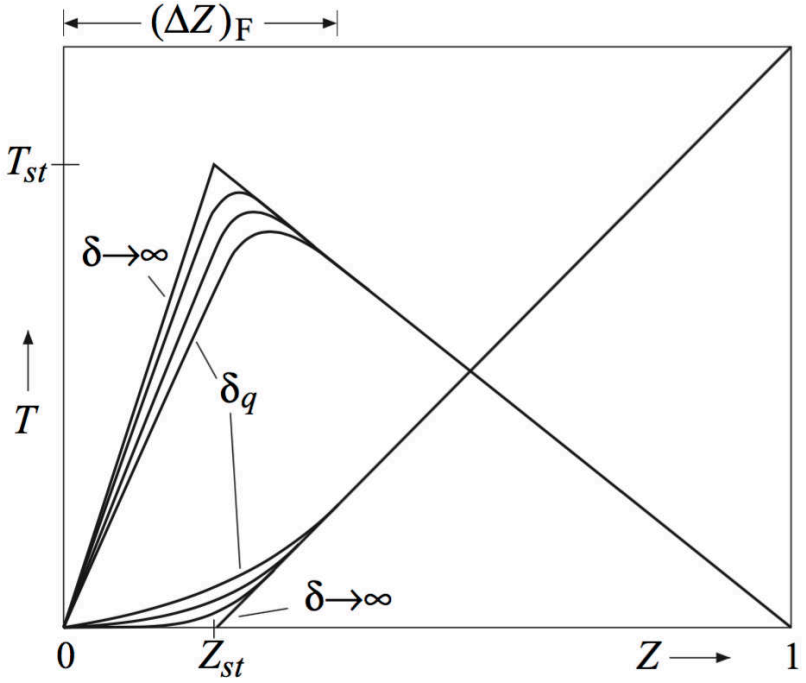

Figure 3: Temperature and fuel mass fraction profiles over mixture fraction for duffusion flamelet

In Figure 3 characteristic profiles for the temperature over Z are schematically shown with δ as a parameter and a limiting profile $T_q(Z)$ corresponding to δ_q. The flamelet would be extinguished because any solution below this profile is unstable. The extinction condition $\delta = \delta_q$ defines a maximum dissipation rate χ_q at the surface of stoichiometric mixture for a flamelet to be burning, namely

Die approbierte gedruckte Originalversion dieser Diplomarbeit ist an der TU Wien Bibliothek verfügbar.
The approved original version of this thesis is available in print at TU Wien Bibliothek.
TU Bibliothek Your knowledge hub WIEN

$$\chi_q = \frac{8B\ \rho_{St}\ \nu'_{O2}\ Y_{F,1}\ Z_{st}^3\ (1-Z_{st})^2}{W_F\ \delta_q\ Ze^3}\ \exp\left(\frac{-E}{R\ T_{st}}\right) \qquad (2.26)$$

χ_{st} is defined as the inverse of a characteristic diffusion time. Heat will be conducted to both sides of the flamelet at a rate that is not balanced by the heat production due to chemical reaction if χ_{st} is large. At a value of $\chi_{st} = \chi_q$ the flamelet is quenched because of a decreased maximum temperature (as shown in Figure 3) where it can be seen that the burning of the flamelet corresponds to the upper branch of the S-shaped curve. The curve is traversed to the left until χ_q is reached, beyond which value only the lower, nonreacting branch exists if χ_{st} is increased. Therefore, the quenching of the diffusion flamelet occurs when $\chi_{st} = \chi_q$ and the transition from the point Q to the lower state corresponds to the unsteady transition. Since the required very large residence times (very small values of χ_{st}) are not reached, auto-ignition is very unlikely to occur in open diffusion flames and would correspond to an unsteady transition from the point I to the upper curve. The combustion in a Diesel engine would be an example for autoignition in non-premixed systems in which inderdiffusion of the fuel from the Diesel spray with the surrounding hot air leads to continuously decreasing mixture fraction gradients and therefore to decreasing scalar dissipation rates so that a shift on the lower branch of the S-shaped curve up to the point I can occur where the ignition takes place. [17]

3. Apparatus and Procedure

Two different configuration setups were employed to carry out experimental studies in order to characterize the critical conditions of the autoignition and extinction events of one hydrocarbon (propane), four alcohols (isobutanol, 1-propanol, ethanol and butane) and two alcohol mixes (n-heptane/isobutanol-mix and n-decane/isobutanol-mix). The first configuration setup is the gaseous counterflow setup and the second configuration is the liquid pool counterflow setup. Both of them can be exchanged as requested (represented with a toggle switch in Figure 4) as shown in the schematic illustration of these two setups in Figure 4. Computer generated mass flow controllers adjust the flow rates of the gases and the temperature of the fuel duct and the oxidizer are measured with thermocouples. The various fuels that were tested and the components of the apparatus are described in detail in the following sections.

Die approbierte gedruckte Originalversion dieser Diplomarbeit ist an der TU Wien Bibliothek verfügbar.
The approved original version of this thesis is available in print at TU Wien Bibliothek.
TU Bibliothek Your knowledge hub WIEN

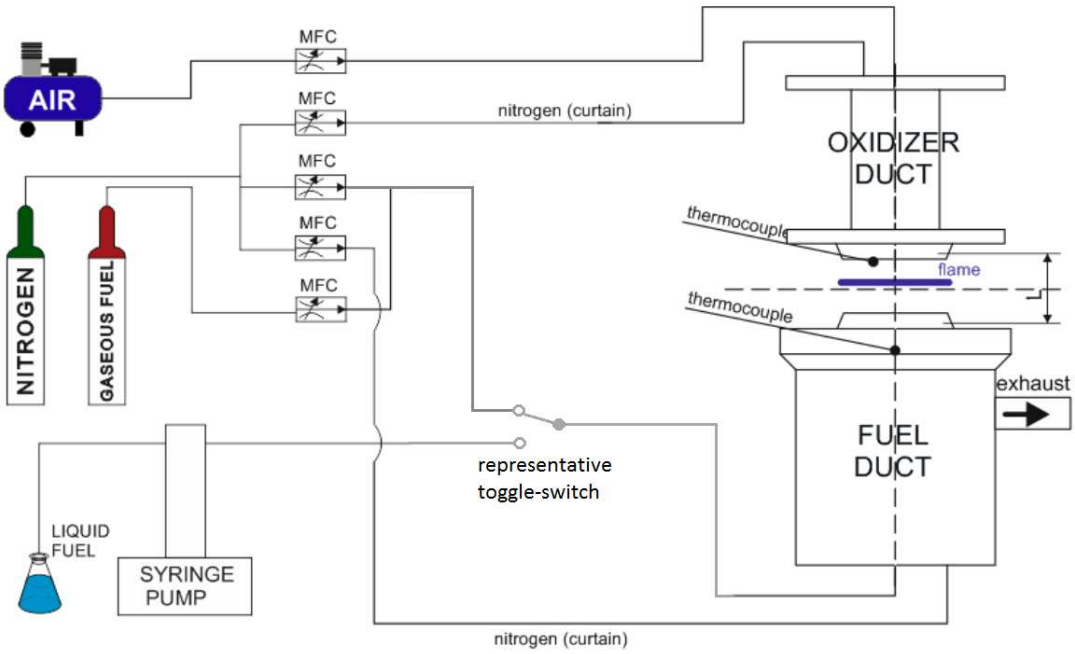

Figure 4: Schematic illustration of the experimental setup, consisting of the counterflow burner, gas and fuel supply and the mass flow controllers

3.1 Tested Fuels

3.1.1 Hydrocarbons

In this thesis the combustion behavior of propane is analyzed. Propane is classified as an organic compound because it contains carbon. It is further categorized as a hydrocarbon because it belongs to a group of organic compounds that are made of only carbon and hydrogen. Hydrocarbons are one oft he most significant classes of organic compounds. A large part of most common used fossil fuels and jet fuels consists of hydrocarbons, in particular hydrocarbons that contain between 6 and 10 carbon atoms [22]. More specifically, propane is a type of hydrocarbon, which is described as an alkane in the literature. The atoms in alkane molecules are held together by single covalent bonds, and carbon atoms always form four covalent bonds. The properties of propane can be found in Table 2.

Die approbierte gedruckte Originalversion dieser Diplomarbeit ist an der TU Wien Bibliothek verfügbar.
The approved original version of this thesis is available in print at TU Wien Bibliothek.

Table 2: Properties of propane [23]

Fuel	Chemical formula	Molar mass [g/mol]	Density at 300 K [kg/m^3]	Boiling point [K]
propane	C_3H_8 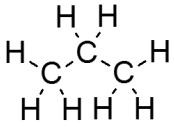	44.097	2.0098	230.9

3.1.2 Alcohols

An alcohol is an organic compound with a hydroxyl (OH) functional group on an aliphatic carbon atom. Because OH is the functional group of all alcohols, we often represent alcohols by the general formula ROH, where R is an alkyl group. Alcohols are common in nature. Most people are familiar with ethyl alcohol (ethanol), the active ingredient in alcoholic beverages, but this compound is only one of a family of organic compounds known as alcohols. The family also includes such familiar substances as cholesterol and the carbohydrates. Methanol (CH_3OH) and ethanol (CH_3CH_2OH) are the first two members of the homologous series of alcohols. The properties of the tested alcohols can be found in Table 3.

Die approbierte gedruckte Originalversion dieser Diplomarbeit ist an der TU Wien Bibliothek verfügbar.
The approved original version of this thesis is available in print at TU Wien Bibliothek.

Table 3: Properties of Isobutanol, 1-Propanol, Ethanol and Butane [24], [25], [26], [27]

fuel	chemical formula	molar mass [g/mol]	density at 300 K [kg/m^3]	boiling point [K]
Isobutanol	$C_4H_{10}O$ 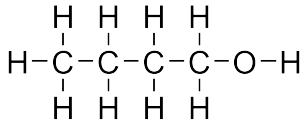	74.122	802	381.04
1-Propanol	C_3H_8O 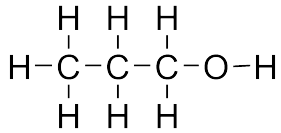	60.096	803	370
Ethanol	C_2H_6O 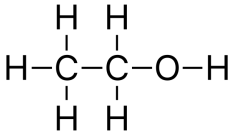	46.069	789.3	351.39
Butane	C_4H_{10} 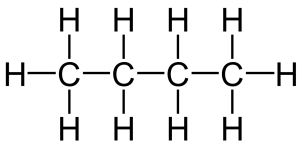	58.124	2.48	273

Die approbierte gedruckte Originalversion dieser Diplomarbeit ist an der TU Wien Bibliothek verfügbar.
The approved original version of this thesis is available in print at TU Wien Bibliothek.

3.2 Counterflow Burner

3.2.1 Lower Part of the Gaseous Counterflow Burner

The aim of the lower part of the burner, which is a complex aluminum construction, is to cool down the exhaust gases with water spray nozzles to prevent further reactions and to guide the gaseous fuel stream into the reaction zone. The fuel stream flows through the main duct into the reaction zone and at the end of this fuel duct three stainless screens are placed which a stainless steel ring separates. In front of these screens a thermocouple is placed on the inlet side to measure the fuel stream temperature before it enters the reaction zone. In order to stabilize the fuel and the oxidizer stream in the reaction zone at the borders, it is important that the curtain duct surrounds the fuel duct and creates co-flow jets of Nitrogen, which also prevents any chemical reactions with ambient air. The internal building extraction system removes the exhaust gases by vacuum. The schematic section view and an image of the burner are shown in Figure 5.

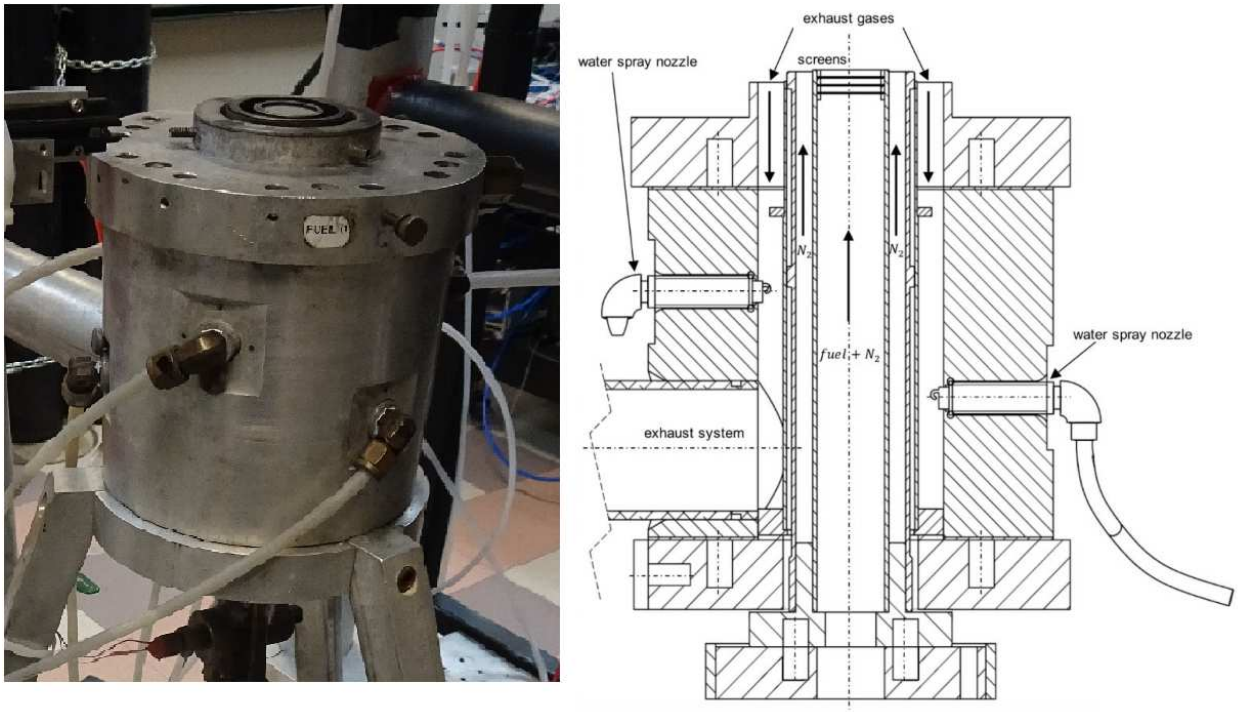

Figure 5: Schematic section view and image of the burner

Die approbierte gedruckte Originalversion dieser Diplomarbeit ist an der TU Wien Bibliothek verfügbar.
The approved original version of this thesis is available in print at TU Wien Bibliothek.

3.2.2 Upper Part of the Counterflow Burner

The most essential part of the experimental setup is the upper part of the burner, which guides the oxidizer stream into the reaction zone. It also produces steady, laminar plug flow conditions, which are the key points in the counterflow theory. Three adjustable pins for setting the separation distance L connect the top with the lower part of the burner. There are two different kinds of tops, which can be used for the counterflow burner as well as for the liquid pool burner. For the extinction experiments an extinction top is used, which is described in 3.2.2.1 and for the autoignition experiments an autoignition top is used, described in 3.2.2.2.

3.2.2.1 Extinction Top

The two main parts of the extinction top are the main duct and the surrounding annular duct. The oxidizer stream is guided by the main duct into the reaction zone and 3 stainless steel screens at the end of the duct form steady laminar flow conditions with axially directed exit velocities. 5 steel rings hold these fine woven stainless steel screens in place, which are made out of Inconel, a material with a high resistance to high temperatures and corrosive environments. Figure 6 shows a screen and an Inconel-ring, which are used at both the autoignition and the extinction top.

The curtain duct guides the nitrogen curtains, which surround the flame to stabilize it and to shield the reactants from the environment with a honeycomb ring close to the end of the duct to ensure plug flow conditions.

Die approbierte gedruckte Originalversion dieser Diplomarbeit ist an der TU Wien Bibliothek verfügbar.
The approved original version of this thesis is available in print at TU Wien Bibliothek.

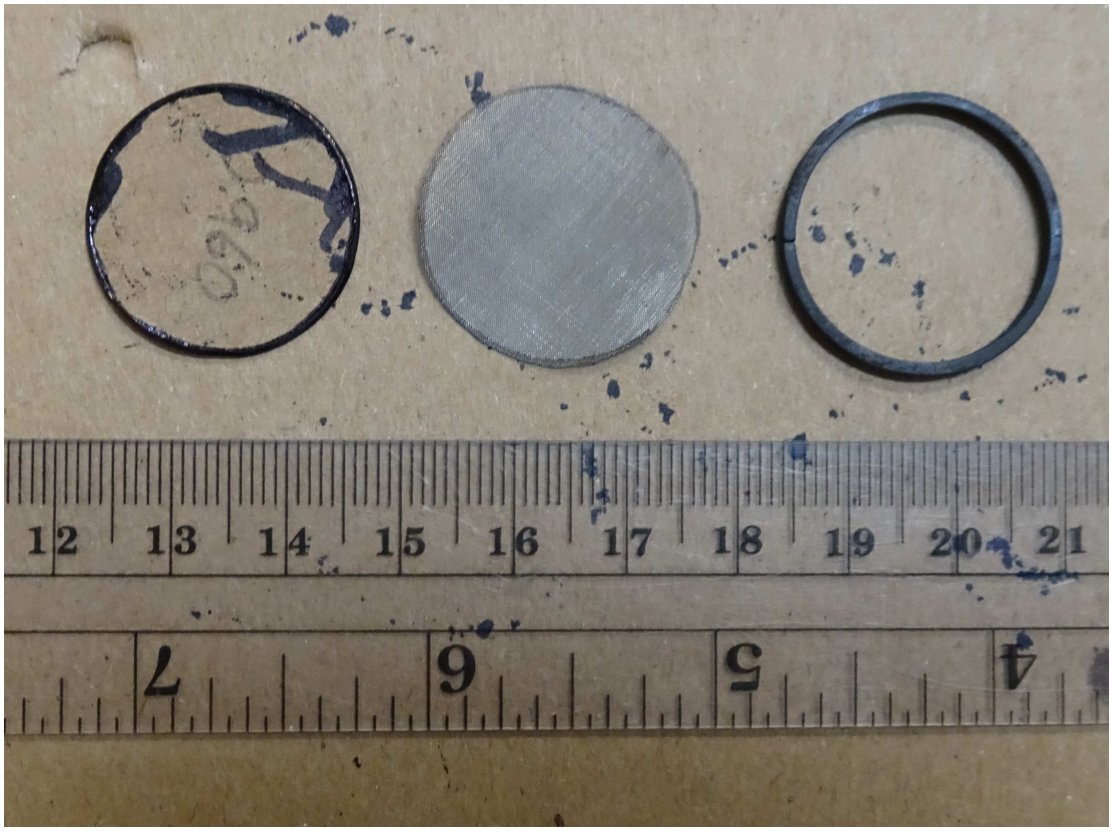

Figure 6: InconelTM 600 gauze 200 screen woven from 0.05 mm diameter wire and an ATI 625™ nickel-based alloy stainless steel ring

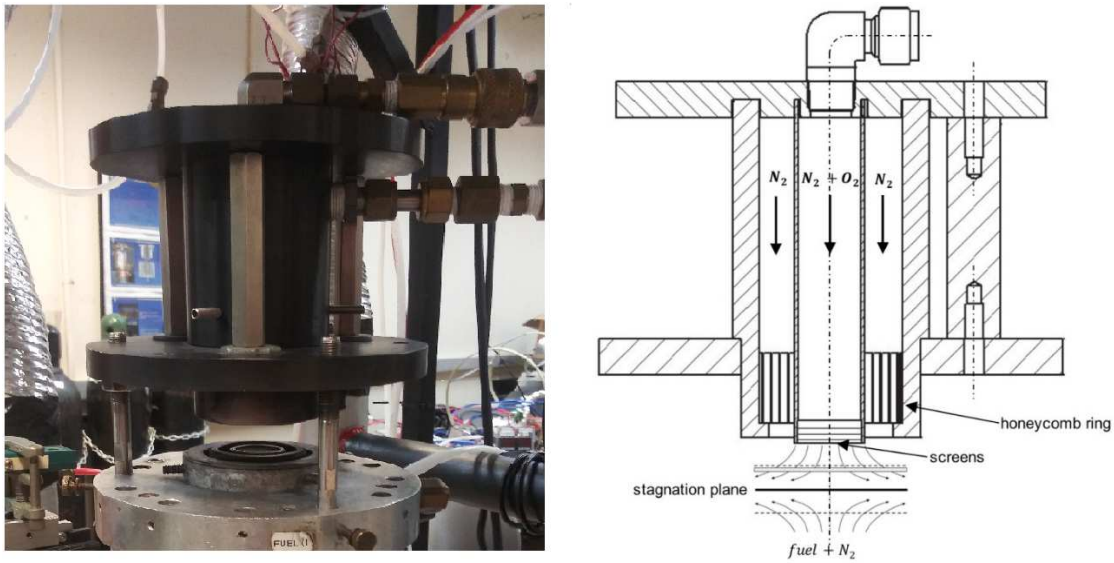

Figure 7: Schematic section view and image of the extinction top

Die approbierte gedruckte Originalversion dieser Diplomarbeit ist an der TU Wien Bibliothek verfügbar.
The approved original version of this thesis is available in print at TU Wien Bibliothek.

3.2.2.2 Autoignition Top

The Starbar®SER silicon carbide heating element is the key part of the autoignition top with two terminal sections called cold ends to heat up the oxidizer stream to the autoignition temperature and a central heating section referred to as a hot zone. Up to 1300 K degrees can be achieved with this heating element, which is surrounded by a quartz oxidizer duct and an annular quartz curtain duct. The autoignition top is provided with a water cooling system to prevent any damage or melting of all the non-ceramic parts and the curtain, furthermore the curtain is isolated with high-temperature Insulfrax® S Blankets. The screens in the autoignition top are the same screens that are being used in the extinction top. The autoignition top is illustrated in Figure 8.

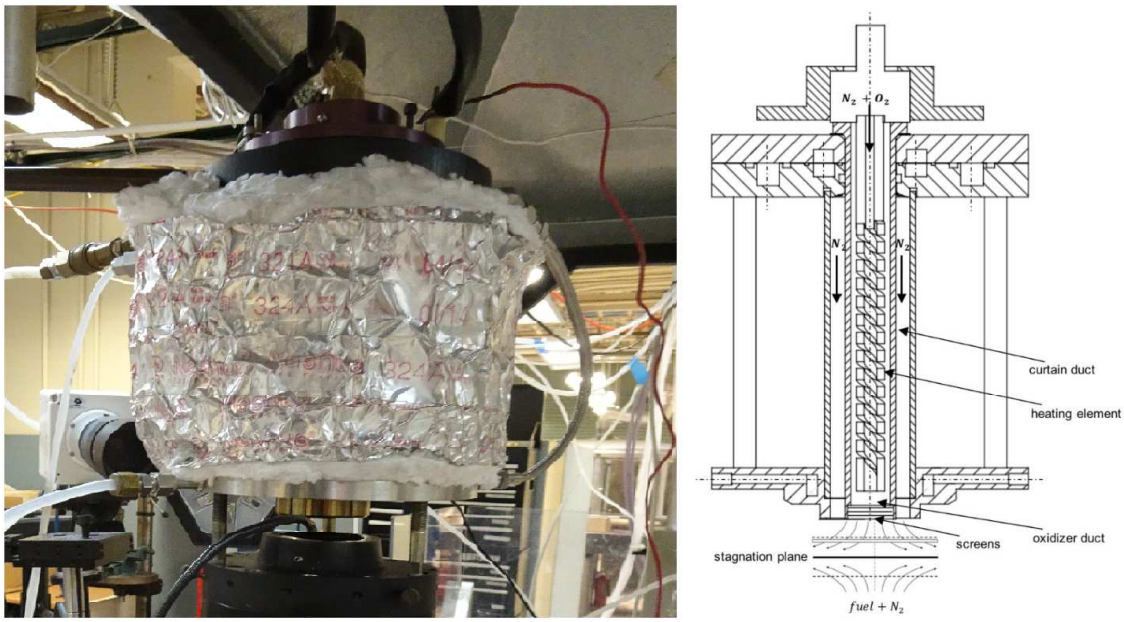

Figure 8: Schematic section view and image of the autoignition top

Die approbierte gedruckte Originalversion dieser Diplomarbeit ist an der TU Wien Bibliothek verfügbar.
The approved original version of this thesis is available in print at TU Wien Bibliothek.

3.3 Liquid Pool Burner

3.3.1 Lower Part of the Liquid Pool Burner

A schematic illustration of the experimental apparatus is shown in figure 9 and it comprises the liquid-fuel burner and the fuel reservoir. Liquid fuel flows from the syringe pump to the fuel-cup and the pump accurately maintains the amount of fuel in the cup at a constant value, by matching the mass rate of fuel flowing from the pump to the fuel-cup to the burning rate. The depth of the fuel cup is 10mm and has an inner diameter of 35mm. A curtain flow of nitrogen flows upward from an annular region and a cooling system surrounds this curtain nitrogen flow. In the mixing-layer between the surface of the liquid pool and the oxidizer-boundary, hot gases that are formed enter this cooling system. Before they enter the exhaust system, the hot gases are cooled by water that is sprayed from a nozzle.

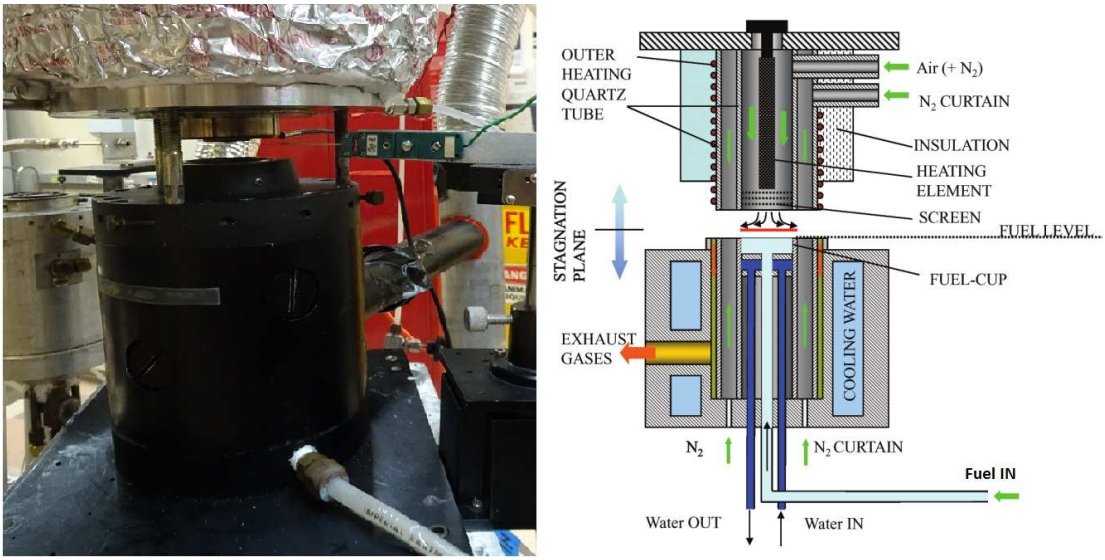

Figure 9: Schematic section view and image of the liquid pool burner

Die approbierte gedruckte Originalversion dieser Diplomarbeit ist an der TU Wien Bibliothek verfügbar.
The approved original version of this thesis is available in print at TU Wien Bibliothek.

3.3.2 Upper Part of the Liquid Pool Burner

The same tops that are used for the counterflow burner (the autoignition top and the extinction top) are used on the liquid pool burner as well and are described in 3.2.2.1 and 3.2.2.2.

3.4 LabView Controlling Software

The entire experimental setup is controlled and monitored with LabView, a visual programming language from National Instruments, which is a control-software that uses a dataflow programming language. This software has been continuously improved and developed over the years. Hardware such as pumps, calibration devices and mass flow controllers are very simple to monitor with the LabView Controlling Software. One liquid reactant and 5 gaseous reactants in each stream can be controlled for the experiments on the counterflow and liquid pool burner. Data such as the oxidizer strain rate (in the upper left), the mass fractions of the fuel stream and oxidizer stream as well as the curtain-flow (lower right) are shown in Figure 10 where the basic control front panel of the VI is shown. Also the different flow-rates of the streams as well as the temperatures of the fuel stream and oxidizer stream can be controlled with this front panel.

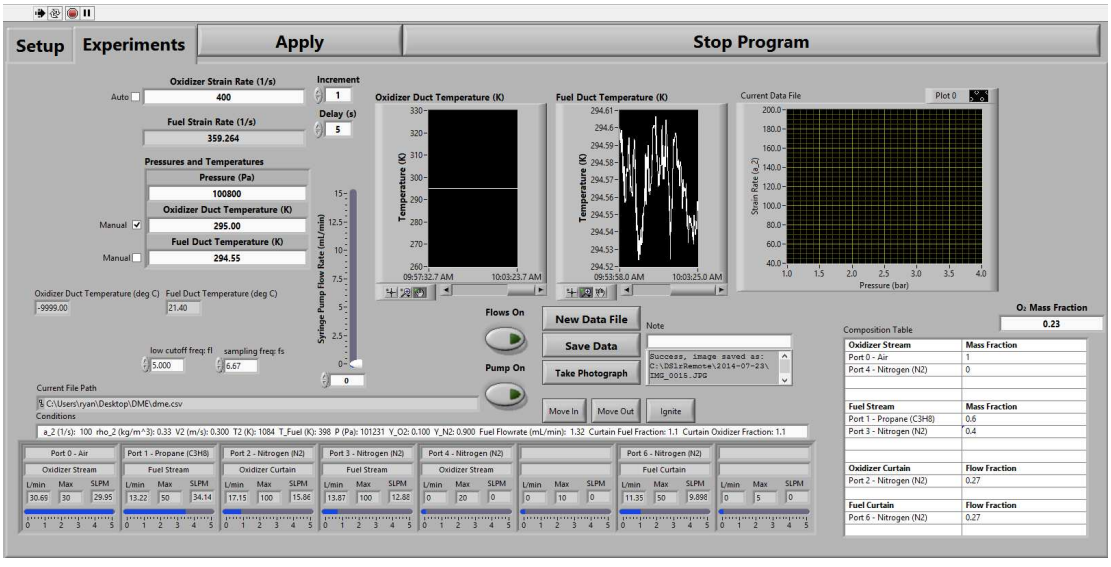

Figure 10: Basic control front panel of the counterflow software

Die approbierte gedruckte Originalversion dieser Diplomarbeit ist an der TU Wien Bibliothek verfügbar.
The approved original version of this thesis is available in print at TU Wien Bibliothek.
TU Bibliothek Your knowledge hub WIEN

It is also necessary to set up all the ports and reactant streams in the main front panel of the software (shown in Figure 10) depending on the needed maximum flow-rates and on the type of the experiment.

3.5 Gas Flow Control and Calibration

Several Teledyne mass flow controllers are used during the experiments with the counterflow and liquid pool burner, which automatically establish and control a stable flow rate of liquids or gases according to a set flow rate sent as an electric signal linear to the mass flow rate. The flow spectrum of the controllers is ranging from 0-50 slm to flows of 0-100 slm and has a full-scale accuracy of about 1%. These mass flow controllers must be calibrated for the maximum flow rate in the respective working range for each individual gas needed in order to obtain results as accurate as possible. A volumetric RITTER Drum-type Gas Meter with a flow range of 0.167 l/min to 33.3 l/min and a National Instruments USB-6008 device is used for the calibration of the mass flow controllers. This measurement device meter works on the principle of displacement and contains a revolving measuring drum within a packing liquid in which the gas can flow through, causing a rotation of the measuring drum within the packaging fluid. Periodically filling and emptying the four rigid measuring chambers, measures the volume of the gas. This periodically filling and emptying makes it possible for the USB device to generate a signal from the counts of the pulses corresponding to the turns of the measuring drum in order to determine the volumetric flow rate. Those conditions and compositions of gases have no influence on the measurement accuracy, which makes the use of this type of gas meter possible because of their direct measurement of volumes. Before each calibration, the level of the packing liquid must be checked carefully to ensure an accurate calibration. The calibration can be controlled using a Labview calibration routine, after the port of the mass flow controller is physically connected to the measurement device. An updated calibration value is calculated and the maximum volumetric flow-rate is directly measured during the calibration. This calibration procedure is repeated until the accuracy of the deviation of the mass flow controllers is less than ±1% and the standard deviation is less than ±0.01%. The front panel of the calibration VI during the calibration procedure is shown in Figure 11, where the deviation of the mass flow controllers should be less than ±1% and the standard deviation less than ±0.01% for a successful calibration.

Die approbierte gedruckte Originalversion dieser Diplomarbeit ist an der TU Wien Bibliothek verfügbar.
The approved original version of this thesis is available in print at TU Wien Bibliothek.
TU Bibliothek Your knowledge hub WIEN

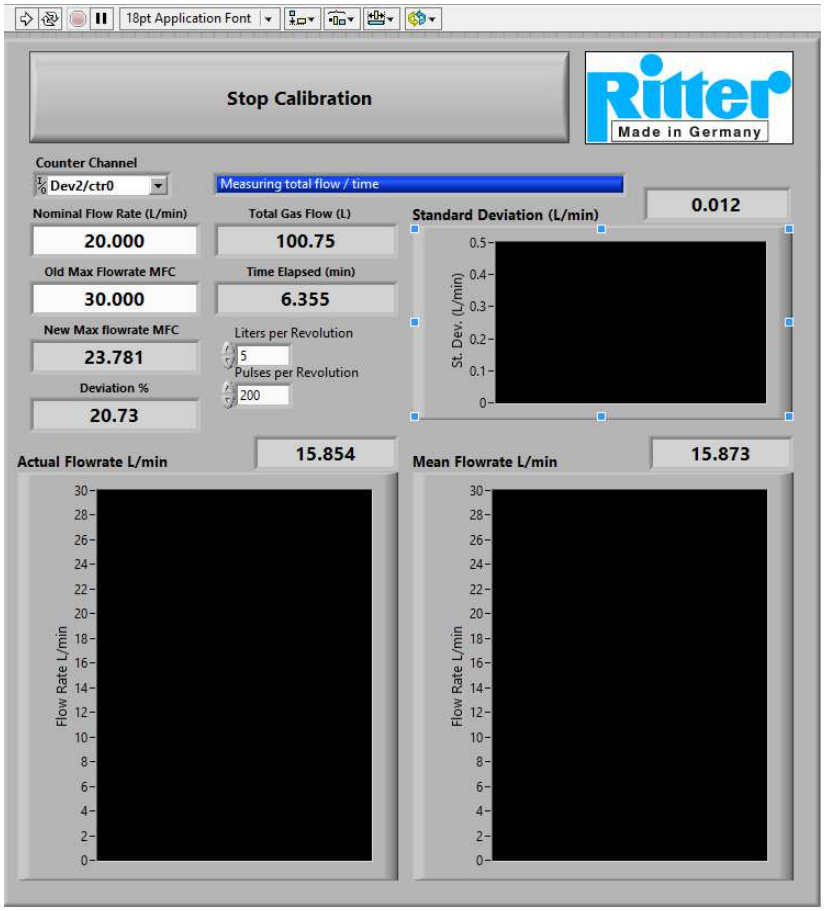

Figure 11: Front panel of the calibration VI during the calibration procedure where the deviation of the mass flow controllers is less than ±1% and the standard deviation is less than ±0.01%.

3.6 Temperature Measurements and Control

A Pt/13%Rh-Pt R-type thermocouple is used to measure the oxidizer stream temperature at the oxidizer exit during the autoignition experiments on the atmospheric counterflow and liquid pool burner. This type of a thermocouple has high service temperatures and stabilities and it is often used for experimental diagnostics in combustion research and in high temperature processes where a quantitative knowledge of the gas temperature is required to determine appropriate kinetic rate constants and to calculate heat fluxes associated with high temperature flows. [28]

Die approbierte gedruckte Originalversion dieser Diplomarbeit ist an der TU Wien Bibliothek verfügbar.
The approved original version of this thesis is available in print at TU Wien Bibliothek.

3.6.1 Temperature Correction

The R-type thermocouple is the most common used thermocouple in laboratory combustion applications to carry out temperature. Considering data evaluation, it is very important to take the radiation losses from the thermocouple from a high temperature gas flow to colder surroundings into account. To avoid those kinds of errors a thermocouple arrangement for combustion-system measurement with the major modes of heat transfer is desired. The following equation gives the energy balance for a thermocouple

$$Q_{cat} + Q_{conv} + Q_{rad} + Q_{cond} = \rho cpV \frac{dT_{tc}}{dt} \text{ [28].} \quad (3.1)$$

It is assumed that the thermocouple is convectively heated by the flow of hot gas and the convective term dominates over all other terms associated with the thermocouple wire and junction [29]. To neglect the catalytic and conduction term, the following assumptions are made:

- high ratio of length to diameter of the thermocouple wire (>200)
- surface-induced catalytic reactions
- small catalytic activity in an air environment

The independency of the wall emissivity with respect for exchange between a gray-emitting thermocouple surface and a much larger, isothermal enclosing diffuse-gray surface [29] is represented by following equation of the surface-area-specific net transport

$$\varepsilon_{tc} \sigma (T_{tc}^4 - T_w^4), \quad (3.2)$$

Hence, the assumption of a steady state environment simplifies equation 3.1 to

$$h(T_g - T_{tc}) = \varepsilon_{tc} \sigma (T_{tc}^4 - T_{surr}^4). \quad (3.3)$$

Die approbierte gedruckte Originalversion dieser Diplomarbeit ist an der TU Wien Bibliothek verfügbar.
The approved original version of this thesis is available in print at TU Wien Bibliothek.
TU Bibliothek Your knowledge hub WIEN

Equation 3.3 can be solved with

$$T_g = T_{tc} + \varepsilon_{tc}\sigma\,(T_{tc}^4 - T_{surr}^4)\,d/kNu. \tag{3.4}$$

for a local gas temperature. Then the radiation loss can be obtained by

$$\Delta = \varepsilon_{tc}\sigma\,(T_{tc}^4 - T_{surr}^4)\,d/kNu \tag{3.5}$$

within 0.02 < *Re* < 44 where Nu represents the Nusselt number for a cylindrical problem with

$$Nu = (0.24+0.56\,Re_d^{0.45})\left(\frac{T_m}{T_\infty}\right)^{17}, \text{ respectively.} \tag{3.6}$$

The Reynolds number is represented by $Re = u2d/v$ with the thermocouple diameter *d,* the viscosity of the oxidizer stream *v* and the oxidizer velocity $u_2 = a_2 * L/4$. In equation 3.5 the second right-handed term is assumed to be 1 [28] [29]. All the parameters needed for the calculation of the radiation losses of the thermocouple at an assumed air oxidizer stream temperature of 1200 [K], are shown in Table 4.

Table 4 Parameter for the calculation of the radiation loss for the oxidizer stream temperature measurements with an R- type thermocouple [28] [30] [31]

T_{surr}	295	[K]	ambient temperature
d	0.0002	[m]	Thermocouple diameter
ε	0.22	[-]	Emissivity for R-Type Themocouple
σ	$5.67 * 10^{-8}$	[W /m^{2}K^4]	Stefan – Boltzmann constant
k	0.0759	[W /mK]	Thermal conductivity
v	0.00015816	[m^2/s]	Kinematic viscosity

Die approbierte gedruckte Originalversion dieser Diplomarbeit ist an der TU Wien Bibliothek verfügbar.
The approved original version of this thesis is available in print at TU Wien Bibliothek.

3.7 Experimental Procedures

3.7.1 Experimental Procedures of the Gaseous Counterflow Burner

- Autoignition with the Gaseous Counterflow Burner at Atmospheric Pressure

Gaseous fuels diluted with nitrogen and an oxidizer stream consisting of pure air is used to measure the critical conditions of autoignition at atmospheric pressure (1.013 bar). The temperature of the oxidizer stream at autoignition as a function of the fuel mass fraction $Y_{F,1}$ at fixed values of $Y_{O2,2}$ = 0.233, and strain rate a_2 = 400 s^{-1} are investigated, as well as the temperature of the oxidizer stream at autoignition as a function of the mass fraction of oxygen $Y_{O2,2}$ at fixed values of $Y_{F,1}$ = 0.21, and strain rate a_2 = 400 s^{-1}. The molecular weight and the density at 300 K of each fuel is entered into the VI for every individual experiment and the mass flow controllers are calibrated for the maximum flow rate in the respective working range for each individual gas before every experimentation in order to obtain accurate results. After calibrating the mass flow controllers, the separation distance between the two ducts is set to 12 mm and the thermocouple is placed as close as possible to the screens at the end of the oxidizer in order to measure the oxidizer stream temperature at autoignition. Before heating up the autoignition top, the cooling system is turned on and a low arbitrary strain rate is set and a flame is established with a blowtorch to control the shape of the flame and the ignitability of the mixture. The autoignition top is heated up very slowly to avoid any thermal stress and damage to the hardware and in order to prevent an overheating of the top, a constant low oxidizer stream, consisting of nitrogen and air, flows through the autoignition top and the lower part of the gaseous conterflow burner. This flow stream also avoids a pure nitrogen atmosphere around the Starbar heating element, which could result in a formation of an insulative silicon nitride layer around the heating element and to over-temperature damage.

The separation distance is checked and adjusted again before the estimated autoignition temperature is reached because of the high heat strain oft he ceramic oxidizer. All streams used are set to their defined values when the expected autoignition temperature is approached and the experiment can start. It is necessary to hold the temperature of the oxidizer as constant as possible in order to investigate the oxidizer stream temperature at a certain point. Then the fuel is injected into the reaction zone for at least 20 seconds to ensure good mixing of the reactants inside the reaction zone. The fuel stream is turned off if no autoignition event occurs. In that case the temperature of the oxidizer stream is increased about 5 [K] and the procedure is repeated again until an autoignition event, shown in Figure 12, occurs. The oxidizer stream temperature is decreased in steps of about 1 [K] after the first autoignition event. The last point where a self-ignition takes place

Die approbierte gedruckte Originalversion dieser Diplomarbeit ist an der TU Wien Bibliothek verfügbar.
The approved original version of this thesis is available in print at TU Wien Bibliothek.

is recorded. This procedure is repeated at least five times for every point to make sure to get the most accurate data possible.

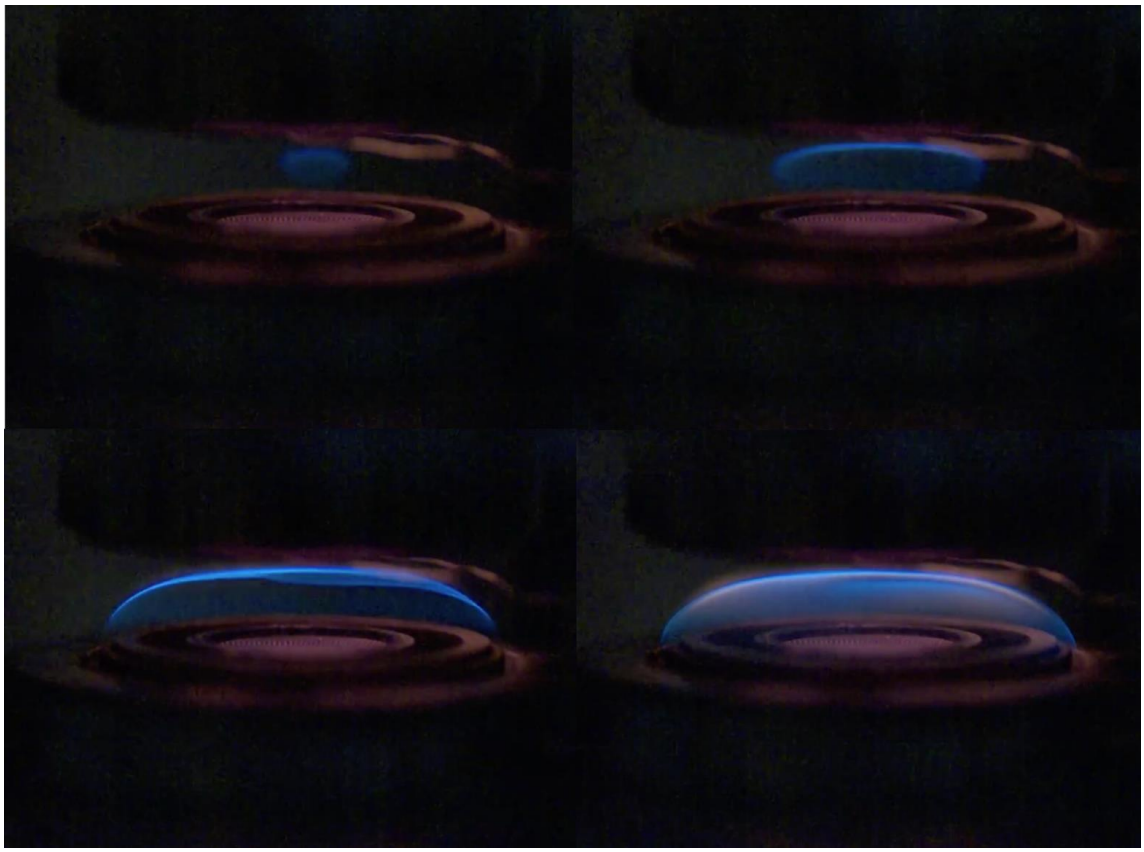

Figure 12: High speed image of an autoignition event with propane with a fuel mass fraction of $Y_{F,1}$ 0.21, oxidizer strain rate a_2 = 400 s^{-1} and pure air as an oxidizer

- Extinction with the Gaseous Counterflow Burner at Atmospheric Pressure

The measurement of the critical conditions of extinction are taking place at an ambient pressure level of 1.013 bar with a liquid fuel and with fixed values of $Y_{O2,2}$ = 0.233 and various values of $Y_{F,1}$. The separation distance between the two ducts is set to 10 mm and the VI is set to the extinction setup before the extinction experiments can be started. Just like in the autoignition experiment the cooling system is turned on and a control flame is established with a blowtorch and held for 10 to 20 seconds. An arbitrary strain rate below the expected extinction strain rate is set and a flame is established with a blowtorch to investigate a specific point. The oxidizer strain rate is increased at a relatively high rate of 10s^{-1} every 5 seconds in order to obtain a rough assessment where the flame will extinguish. A new strain

Die approbierte gedruckte Originalversion dieser Diplomarbeit ist an der TU Wien Bibliothek verfügbar.
The approved original version of this thesis is available in print at TU Wien Bibliothek.
TU Bibliothek Your knowledge hub WIEN

rate below the first extinction strain rate is set as soon as the flame extinguishes. Then the oxidizer strain rate is increased at a rate of $5s^{-1}$ every 5 seconds and the strain rate where the flame extinguishes for the second time is recorded so that the mass flow controllers can be calibrated for this flow rate in this working range for every gas used in the experiment. After that, a strain rate close to the extinction strain rate is set and a flame established, so that the strain rate can be increased with a rate of $1s^{-1}$ every 8 seconds until the flame extinguishes. This procedure is also repeated at least five times for every point to obtain results as accurate as possible. Figure 13 shows the flame during an extinction event of propane.

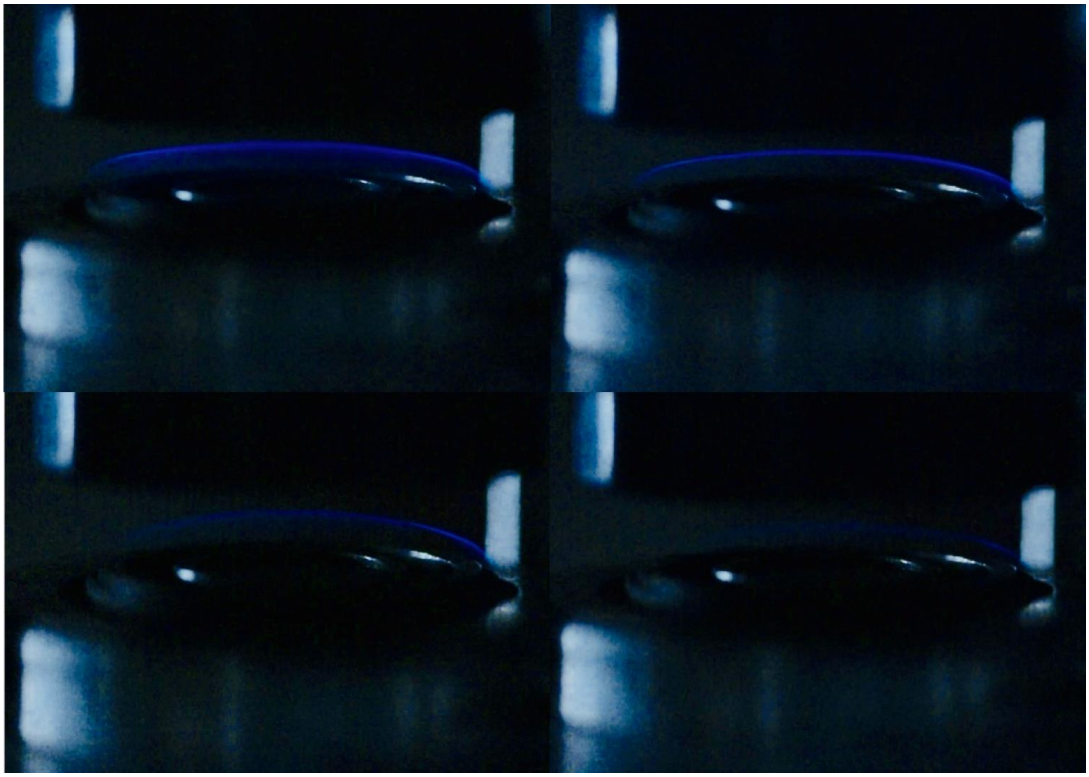

Figure 13: High speed image of an extinction event with propane with a fuel mass fraction of $Y_{F,1}$ = 0.6, oxidizer strain rate a_2 = 366 s^{-1} and pure air as an oxidizer

3.7.2 Experimental Procedures of the Liquid Pool Counterflow Burner

- Autoignition at Atmospheric Pressure with the Liquid Pool Counterflow Burner

The critical conditions of autoignition with the liquid pool counterflow burner at atmospheric pressure (1.013 bar) are measured with liquid fuels and an oxidizer stream consisting of oxygen and nitrogen. The temperature of the oxidizer stream at

Die approbierte gedruckte Originalversion dieser Diplomarbeit ist an der TU Wien Bibliothek verfügbar.
The approved original version of this thesis is available in print at TU Wien Bibliothek.
TU Bibliothek Your knowledge hub WIEN

autoignition as a function of the strain rate a_2 at fixed values of $Y_{O2,2}$ = 0.233 are investigated. The separation distance between the two ducts is set to 12 mm and the syringe pump is flushed and filled with the fuel being examined. As in the two experiments before, the cooling system is turned on and the thermocouple is placed as close to the screens of the oxidizer duct as possible. In order to be able to make sure that the flame has the required shape for the experiment, a low arbitrary strain rate is set to establish the test-flame. The heating of the autoignition top is handled the same way as in the autoignition experiment with the gaseous counterflow burner, except that the fuel cup has to be filled with the fuel that is being examined and the level of the fuel in it has to be constant during the heating of the top. Once an autoignition event occurs the temperature of the oxidizer stream is noted and the flame is extinguished with an increase in nitrogen in the oxidizer stream. Then the autoignition top is cooled down to a temperature below the first autoignition event and heated up again with the oxygen mass fraction of $Y_{O2,2}$ = 0.233 so that the experiment can be repeated for the same temperature point. This procedure is repeated at least five times for every temperature point to make sure to get the most accurate results as possible. Figure 14 shows the flame during an autoignition event of heptane.

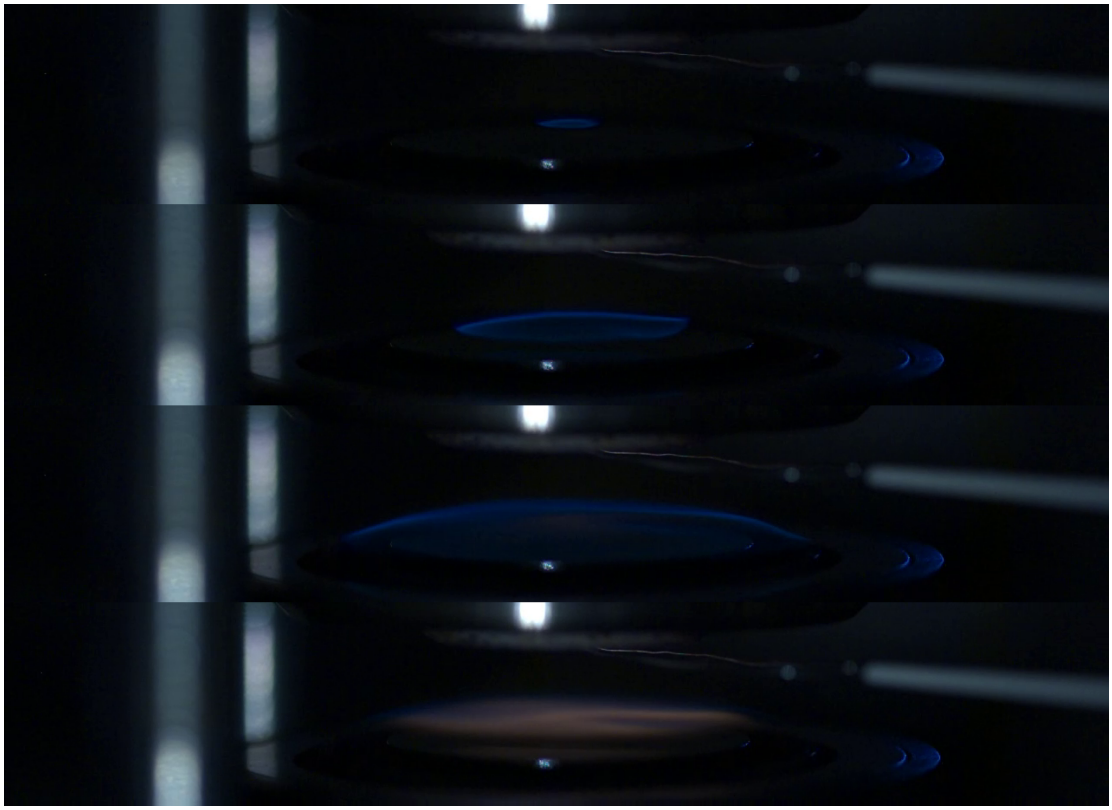

Figure 14: High speed image of an autoignition event with heptane with an oxidizer strain rate a_2 = 150 s^{-1} and pure air as an oxidizer

Die approbierte gedruckte Originalversion dieser Diplomarbeit ist an der TU Wien Bibliothek verfügbar.
The approved original version of this thesis is available in print at TU Wien Bibliothek.

4 Discussions of the Experimental Results of the Atmospheric Pressure Counterflow Burner

Chapter 4 summarizes the experimental results. The detailed numerical results of the experiments shown in the following chapters are attached in the appendix.

4.1 Discussions of the Experimental Results of the Gaseous Counterflow Burner

4.1.1 Results of the Autoignition Experiments

The autoignition experiments were carried out with propane at different fuel stream temperatures to investigate the influence of different fuel- and oxygen mass fractions on the autoignition event. The experiments with different fuel mass fractions were conducted from the lowest fuel mass fraction of $Y_{F,1}$ = 0.3 to the highest fuel mass fraction of $Y_{F,1}$ = 0.6. The experiments with different oxygen mass fractions were conducted from the lowest oxygen mass fraction of $Y_{O2,2}$ = 0.07 to the highest oxygen mass fraction of $Y_{O2,2}$ = 0.233. The displayed experimental data points are arithmetically averaged values and all results are corrected due to radiation losses.

Figure 15 shows the temperature of the oxidizer stream at autoignition $T_{2,ign}$, as a function of the mass fraction of oxygen $Y_{O2,2}$ for propane.

The higher the oxygen mass fraction, the more oxygen and therefore less nitrogen is in the oxidizer stream respectively in the reaction zone. Nitrogen is non-flammable and mainly used to stabilize the flame. Oxygen is an oxidizer, which means it supports the process of combustion, as it is shown in the following basic chemical reaction for the combustion of propane:

- $2\ C_3H_8 + 7O_2 \rightarrow 6\ CO_2 + 8\ H_2O$

Die approbierte gedruckte Originalversion dieser Diplomarbeit ist an der TU Wien Bibliothek verfügbar.
The approved original version of this thesis is available in print at TU Wien Bibliothek.

So the higher the oxygen mass fraction (more oxygen and less nitrogen in the reaction zone), the lower the autoignition temperature.

The results in in figure 15 show these characteristics pretty well. As expected the autoignition temperature decreases with an increasing oxygen mass fraction because of the increasing ratio of propane and the decreasing ratio of nitrogen in the reaction zone.

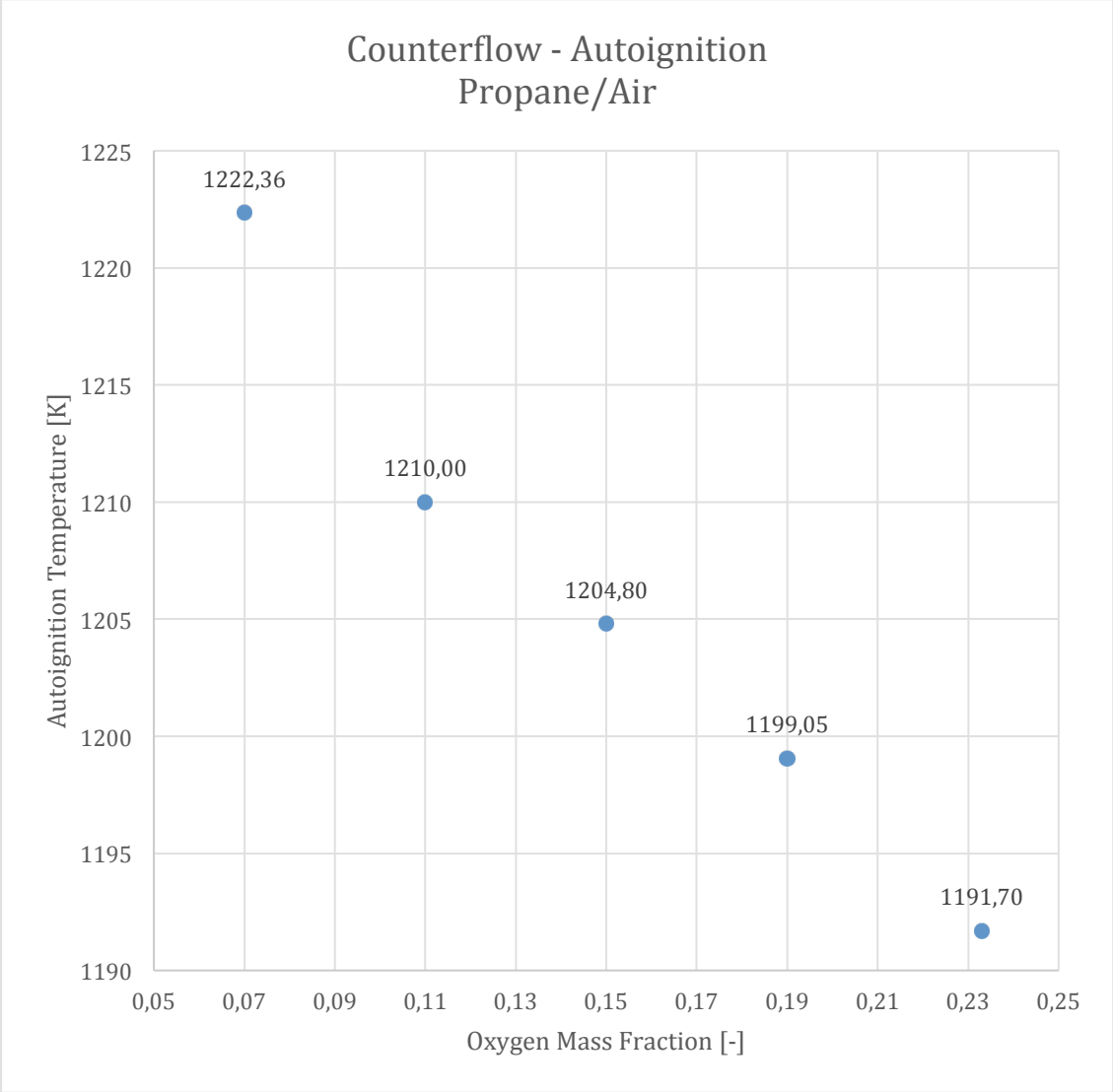

Figure 15: The temperature of the oxidizer stream at autoignition $T_{2,ign}$ as a function of the mass fraction of oxygen $Y_{O2,2}$ for $Y_{F,1}$ = 0.21, T_1 = 294.15 [K] and a_2 = 400 s^{-1}

Die approbierte gedruckte Originalversion dieser Diplomarbeit ist an der TU Wien Bibliothek verfügbar.
The approved original version of this thesis is available in print at TU Wien Bibliothek.

Figure 16 illustrates the temperature of the oxidizer stream at autoignition $T_{2,ign}$ as a function of the mass fraction of fuel $Y_{F,1}$ for propane.

The higher the fuel mass fraction, the more propane and therefore less nitrogen is in the fuel stream respectively in the reaction zone. Since propane is highly flammable and nitrogen is non-flammable and mainly used to stabilize the flame, a lower temperature is needed to start an ignition if the fuel mass fraction and therefore the ratio of propane in the reaction zone increases and the ratio of nitrogen in the reaction zone decreases. So the higher the fuel mass fraction ratio (more propane and less nitrogen in the reaction zone) the lower the autoignition temperature.

The results in figure 16 show this characteristic pretty well. As expected the autoignition temperature decreases with increasing fuel mass fraction because of the increasing ratio of nitrogen and the decreasing ratio of propane.

It also shows that the variation of the fuel mass fraction has a similar influence on the autoignition temperature compared to the variation of the oxygen mass fraction in figure 15. So both experiments show a similar characteristic.

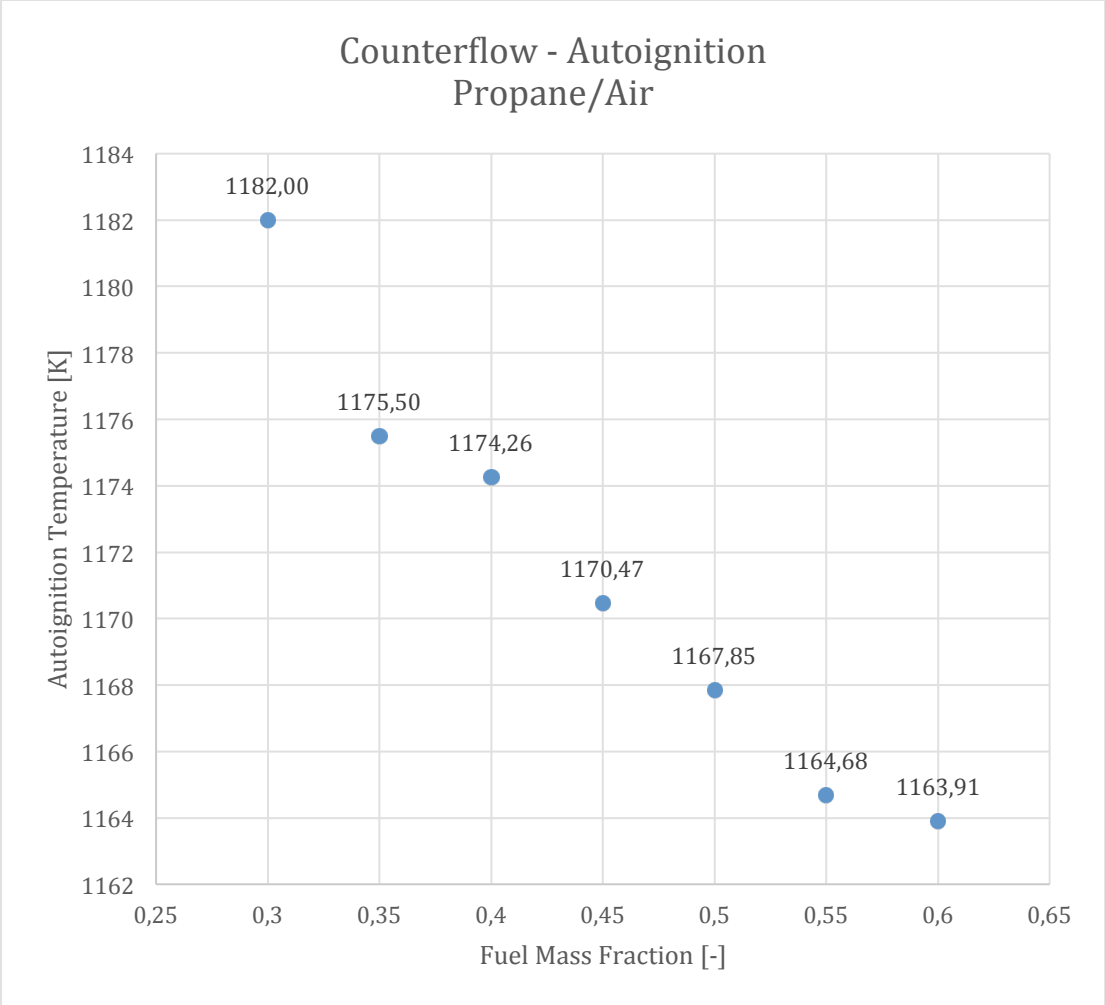

Figure 16: The temperature of the oxidizer stream at autoignition $T_{2,ign}$ as a function of the mass fraction of fuel $Y_{F,1}$ for $Y_{O2,2}$ = 0.23, T1 = 294.15 [K] and a_2 = 400 s^{-1}

Die approbierte gedruckte Originalversion dieser Diplomarbeit ist an der TU Wien Bibliothek verfügbar.
The approved original version of this thesis is available in print at TU Wien Bibliothek.
TU Bibliothek Your knowledge hub WIEN

4.1.2 Results of the Extinction Experiments

The extinction experiments were carried out to investigate the influence of different oxygen mass fractions Y_{O2} on the critical conditions of extinction. The experiments with different oxygen mass fractions were conducted from the lowest oxygen mass fraction of $Y_{O2,2} = 0.195$ to the highest fuel mass fraction of $Y_{O2,2} = 0.5$. The displayed experimental data points are arithmetically averaged values.

Figure 17 shows the experimental results for propane at different oxygen mass fractions of fuel $Y_{O2,2}$ as a function of the strain rate at extinction.

The higher the oxygen mass fraction, the more oxygen and therefore less nitrogen is in the oxidizer stream respectively in the reaction zone. Nitrogen is non-flammable and mainly used to stabilize the flame. Oxygen is an oxidizer, which means it supports the process of combustion, as it is shown in the following basic chemical reaction for the combustion of propane:

- $2\ C_3H_8 + 7O_2 \rightarrow 6\ CO_2 + 8\ H_2O$

So the higher the oxygen mass fraction (more oxygen and less nitrogen in the reaction zone), the higher the strain rate on where the flame goes extinct.

The results in in figure 17 show these characteristics pretty well. As expected the strain rate increases with an increasing oxygen mass fraction because of the increasing ratio of propane and the decreasing ratio of nitrogen in the reaction zone.

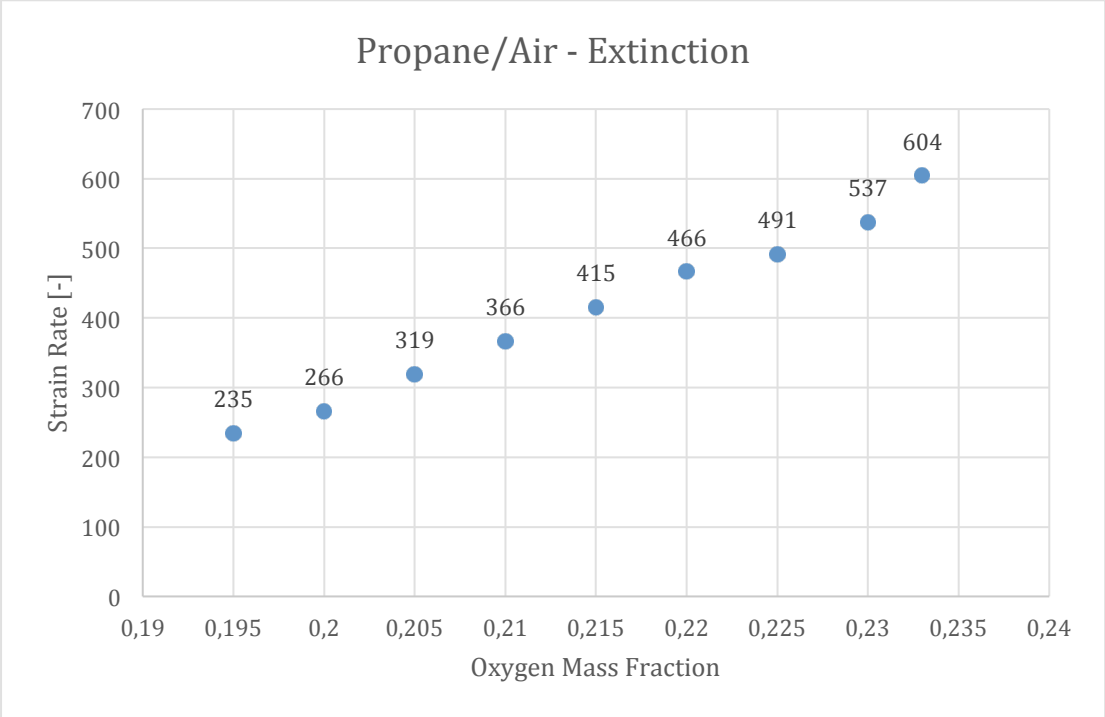

Figure 17: The extinction strain rate a_2 as a function of the oxygen mass fraction $Y_{O2,2}$ for T = 294.15 [K].

Die approbierte gedruckte Originalversion dieser Diplomarbeit ist an der TU Wien Bibliothek verfügbar.
The approved original version of this thesis is available in print at TU Wien Bibliothek.
TU Bibliothek Your knowledge hub WIEN

4.2 Discussion of the Experimental Results of the Liquid Pool Counterflow Burner

4.2.1 Results of the Autoignition Experiments

The autoignition experiments with liquid fuels were carried out with n-heptane, isobutanol, isobutanol/n-heptane - mix, 1-propanol, ethanol, n-decane, isobutanol/n-decane - mix and butane at different strain rates to investigate the influence of different strain rates on the autoignition temperature. These experiments were conducted from the lowest strain rate of a_2 = 100 s^{-1} to the highest strain rate of a_2 = 450 s^{-1}. The displayed experimental data points are arithmetically averaged values and all results are corrected due to radiation losses.

Figure 18 shows the temperature of the oxidizer stream at autoignition $T_{2,ign}$ as a function of the strain rate a_2 for heptane.

The strain rate is defined as the axial flow, in other words it can be described as the reciprocal of the characteristic flow time given by the equation

$$a_2 = 2V_2 / L \qquad [32]$$

So the higher the strain rate of the oxidizer stream, the higher the velocity of the oxidizer stream ($Y_{O2,2}$ = 0.23) flowing through the reaction zone where the ignition takes place.

In order to start an ignition it is important that the reactants (the air of the oxidizer stream and the vapor of the liquid fuel) can mix properly and it is also essential that there is enough time for the ignition-reaction to take place. This means that a high strain rate, respectively a high velocity of the oxidizer stream through the reaction zone can lead to conditions where it is harder to ignite a flame. In other words a higher strain rate can lead to a higher autoignition temperature.

The results in figure 18 show these characteristics pretty well. As expected the autoignition temperature increases with an increasing strain rate.

Die approbierte gedruckte Originalversion dieser Diplomarbeit ist an der TU Wien Bibliothek verfügbar.
The approved original version of this thesis is available in print at TU Wien Bibliothek.

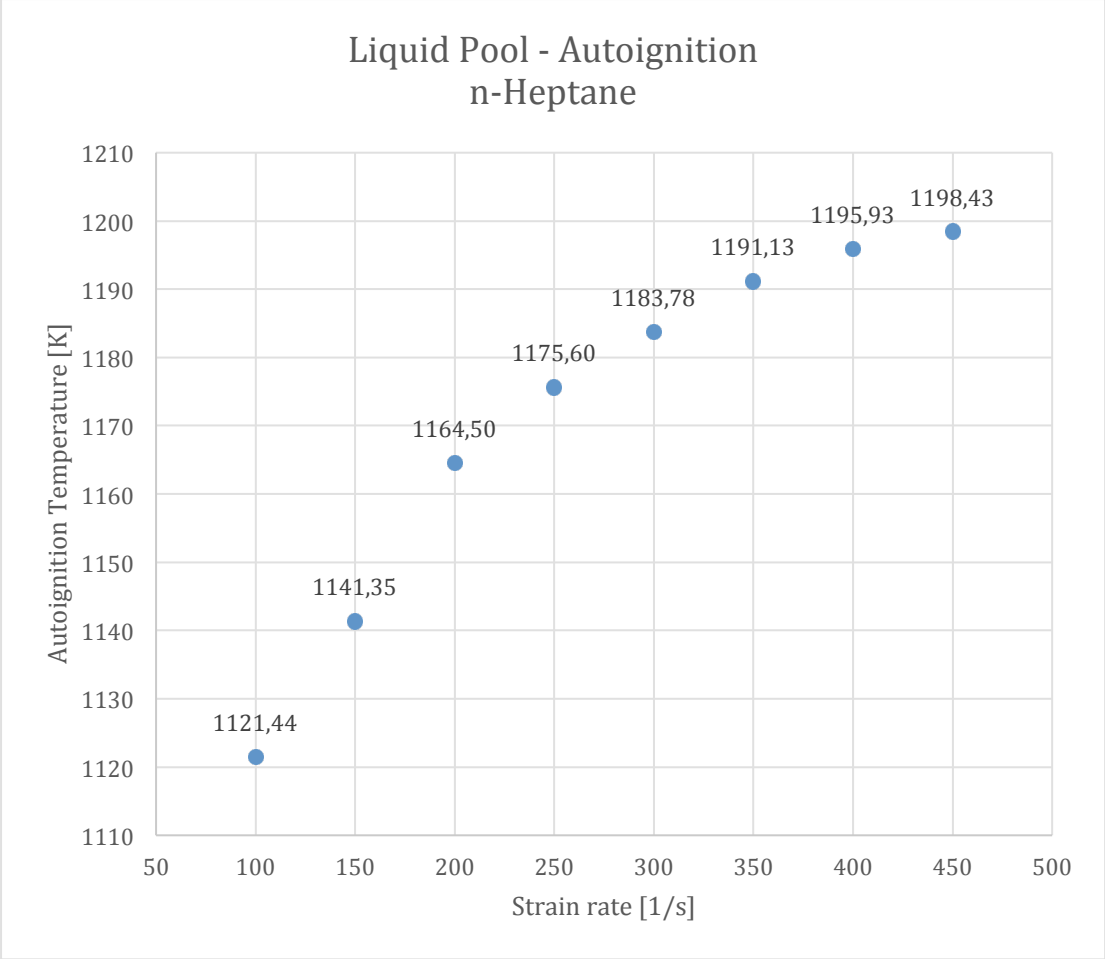

Figure 18: The temperature of the oxidizer stream at autoignition $T_{2,ign}$ as a function of the strain rate a_2 for $Y_{O2,2} = 0.23$, $T_1 = 294.15$ [K]

Figure 19 shows the temperature of the oxidizer stream at autoignition $T_{2,ign}$ as a function of the strain rate a_2 for isobutanol.

The strain rate is defined as the axial flow, in other words it can be described as the reciprocal of the characteristic flow time.

So the higher the strain rate of the oxidizer stream, the higher the velocity of the oxidizer stream ($Y_{O2,2} = 0.23$) flowing through the reaction zone where the ignition takes place.

In order to start an ignition it is important that the reactants (the air of the oxidizer stream and the vapor of the liquid fuel) can mix properly and it is also essential that there is enough time for the ignition-reaction to take place. This means that a high strain rate, respectively a high velocity of the oxidizer stream through the reaction zone can lead to conditions where it is harder to ignite a flame. In other words a higher strain rate can lead to a higher autoignition temperature.

Die approbierte gedruckte Originalversion dieser Diplomarbeit ist an der TU Wien Bibliothek verfügbar.
The approved original version of this thesis is available in print at TU Wien Bibliothek.
TU Bibliothek Your knowledge hub WIEN

The results in figure 19 show these characteristics pretty well. As expected the autoignition temperature increases with an increasing strain rate.

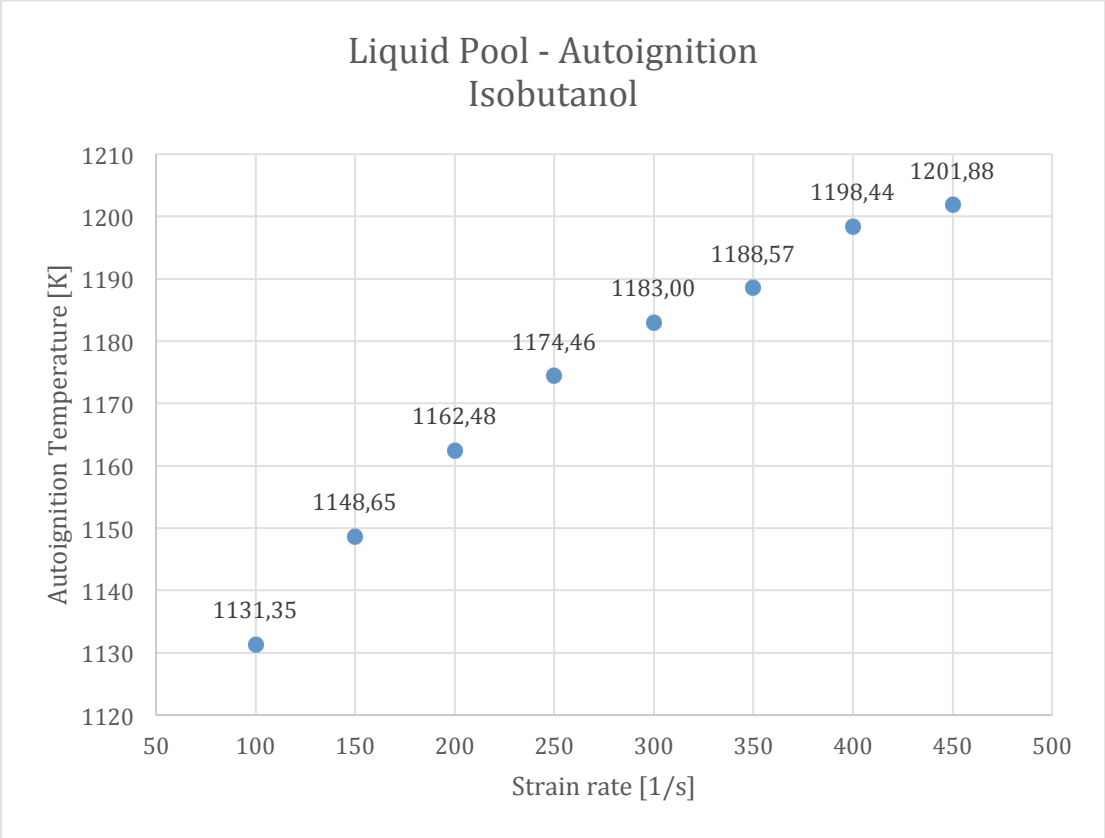

Figure 19: The temperature of the oxidizer stream at autoignition, $T_{2,ign}$ as a function of the strain rate a_2 for $Y_{O2,2} = 0.23$, $T_1 = 294.15$ [K]

Figure 20 shows the temperature of the oxidizer stream at autoignition $T_{2,ign}$ as a function of the strain rate a_2 for a 50% to 50% mix between isobutanol and n-heptane.

The strain rate is defined as the axial flow, in other words it can be described as the reciprocal of the characteristic flow time.

So the higher the strain rate of the oxidizer stream, the higher the velocity of the oxidizer stream ($Y_{O2,2} = 0.23$) flowing through the reaction zone where the ignition takes place.

In order to start an ignition it is important that the reactants (the air of the oxidizer stream and the vapor of the liquid fuel) can mix properly and it is also essential that there is enough time for the ignition-reaction to take place. This means that a high strain rate, respectively a high velocity of the oxidizer stream through the reaction

Die approbierte gedruckte Originalversion dieser Diplomarbeit ist an der TU Wien Bibliothek verfügbar.
The approved original version of this thesis is available in print at TU Wien Bibliothek.
TU Bibliothek Your knowledge hub WIEN

zone can lead to conditions where it is harder to ignite a flame. In other words a higher strain rate can lead to a higher autoignition temperature.

The results in figure 20 show these characteristics pretty well. As expected the autoignition temperature increases with an increasing strain rate.

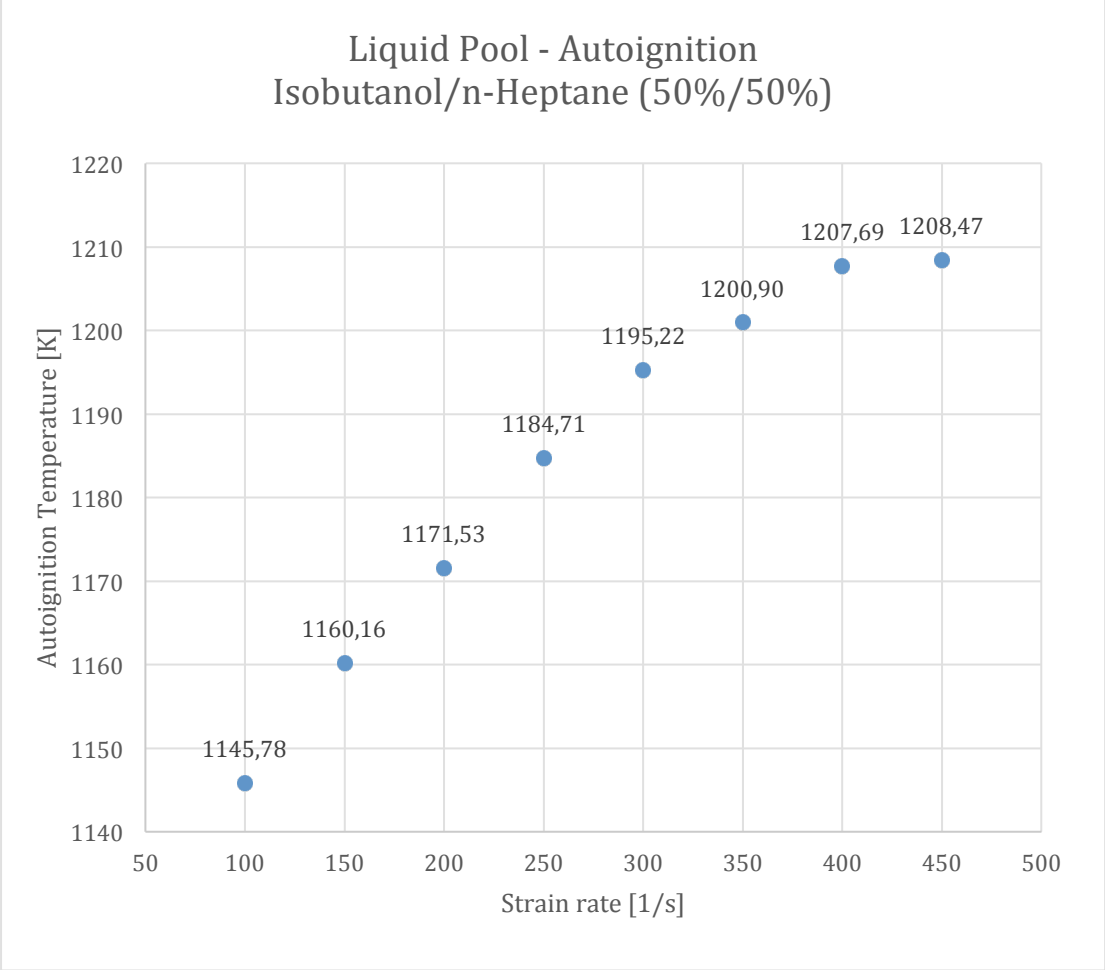

Figure 20: The temperature of the oxidizer stream at autoignition, $T_{2,ign}$ as a function of the strain rate a_2 for $Y_{O2,2}$ = 0.23, T_1 = 294.15 [K]

Figure 21 shows the temperature of the oxidizer stream at autoignition $T_{2,ign}$ as a function of the strain rate a_2 for 1-propanol.

The strain rate is defined as the axial flow, in other words it can be described as the reciprocal of the characteristic flow time.

So the higher the strain rate of the oxidizer stream, the higher the velocity of the oxidizer stream ($Y_{O2,2}$ = 0.23) flowing through the reaction zone where the ignition takes place.

Die approbierte gedruckte Originalversion dieser Diplomarbeit ist an der TU Wien Bibliothek verfügbar.
The approved original version of this thesis is available in print at TU Wien Bibliothek.

In order to start an ignition it is important that the reactants (the air of the oxidizer stream and the vapor of the liquid fuel) can mix properly and it is also essential that there is enough time for the ignition-reaction to take place. This means that a high strain rate, respectively a high velocity of the oxidizer stream through the reaction zone can lead to conditions where it is harder to ignite a flame. In other words a higher strain rate can lead to a higher autoignition temperature.

The results in figure 21 show these characteristics pretty well. As expected the autoignition temperature increases with an increasing strain rate.

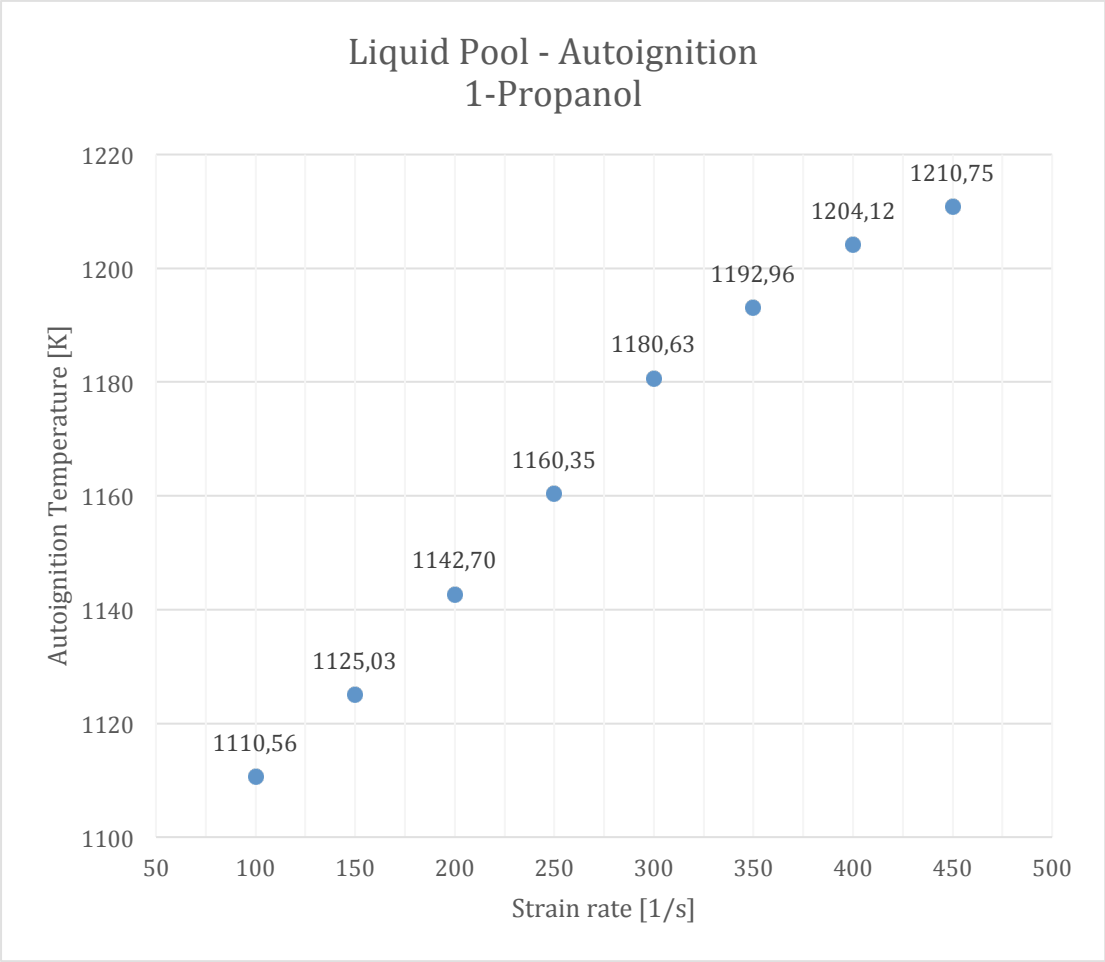

Figure 21: The temperature of the oxidizer stream at autoignition, $T_{2,ign}$ as a function of the strain rate a_2 for $Y_{O2,2} = 0.23$, $T_1 = 294.15$ [K]

Figure 22 shows the temperature of the oxidizer stream at autoignition $T_{2,ign}$ as a function of the strain rate a_2 for ethanol.

The strain rate is defined as the axial flow, in other words it can be described as the reciprocal of the characteristic flow time.

Die approbierte gedruckte Originalversion dieser Diplomarbeit ist an der TU Wien Bibliothek verfügbar.
The approved original version of this thesis is available in print at TU Wien Bibliothek.

So the higher the strain rate of the oxidizer stream, the higher the velocity of the oxidizer stream ($Y_{O2,2}$ = 0.23) flowing through the reaction zone where the ignition takes place.

In order to start an ignition it is important that the reactants (the air of the oxidizer stream and the vapor of the liquid fuel) can mix properly and it is also essential that there is enough time for the ignition-reaction to take place. This means that a high strain rate, respectively a high velocity of the oxidizer stream through the reaction zone can lead to conditions where it is harder to ignite a flame. In other words a higher strain rate can lead to a higher autoignition temperature.

The results in figure 22 show these characteristics pretty well. As expected the autoignition temperature increases with an increasing strain rate.

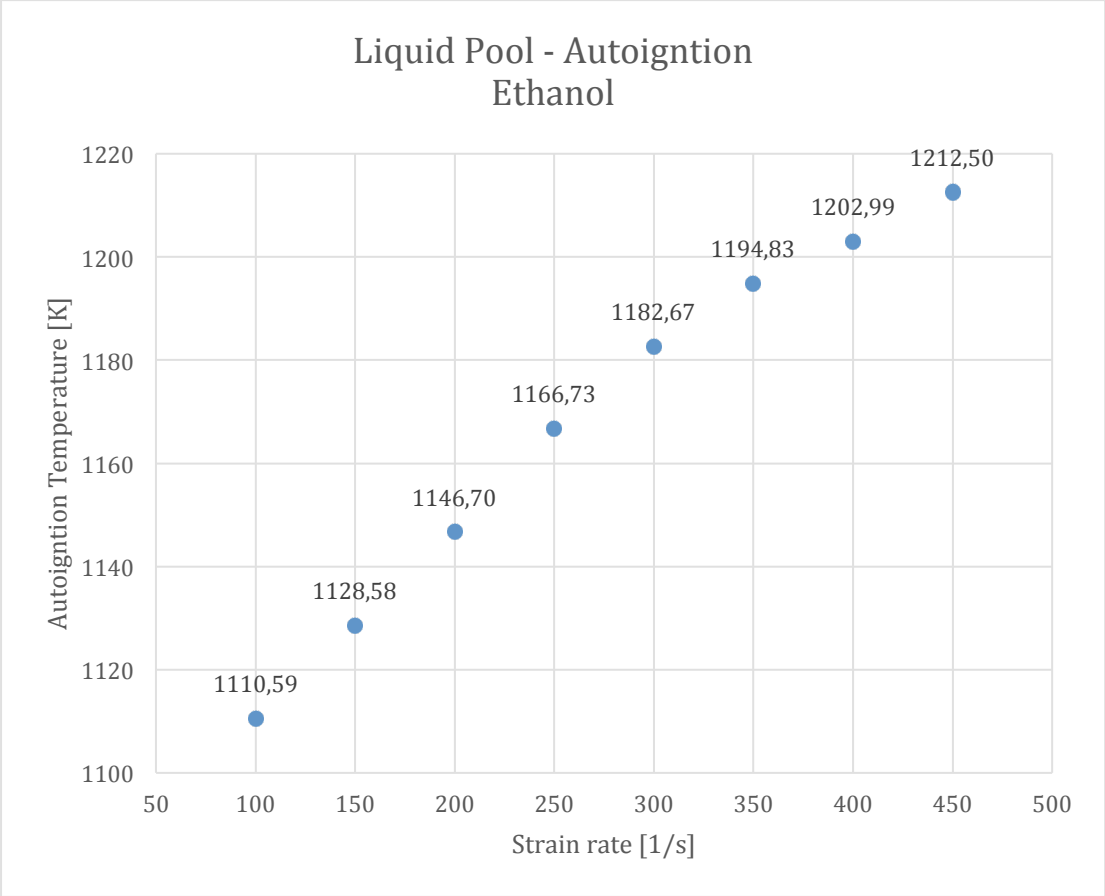

Figure 22: The temperature of the oxidizer stream at autoignition $T_{2,ign}$ as a function of the strain rate a_2 for $Y_{O2,2}$ = 0.23, T_1 = 294.15 [K]

Figure 23 shows the temperature of the oxidizer stream at autoignition $T_{2,ign}$ as a function of the strain rate a_2 for n-decane.

Die approbierte gedruckte Originalversion dieser Diplomarbeit ist an der TU Wien Bibliothek verfügbar.
The approved original version of this thesis is available in print at TU Wien Bibliothek.

The strain rate is defined as the axial flow, in other words it can be described as the reciprocal of the characteristic flow time.

So the higher the strain rate of the oxidizer stream, the higher the velocity of the oxidizer stream ($Y_{O2,2}$ = 0.23) flowing through the reaction zone where the ignition takes place.

In order to start an ignition it is important that the reactants (the air of the oxidizer stream and the vapor of the liquid fuel) can mix properly and it is also essential that there is enough time for the ignition-reaction to take place. This means that a high strain rate, respectively a high velocity of the oxidizer stream through the reaction zone can lead to conditions where it is harder to ignite a flame. In other words a higher strain rate can lead to a higher autoignition temperature.

The results in figure 23 show these characteristics pretty well. As expected the autoignition temperature increases with an increasing strain rate.

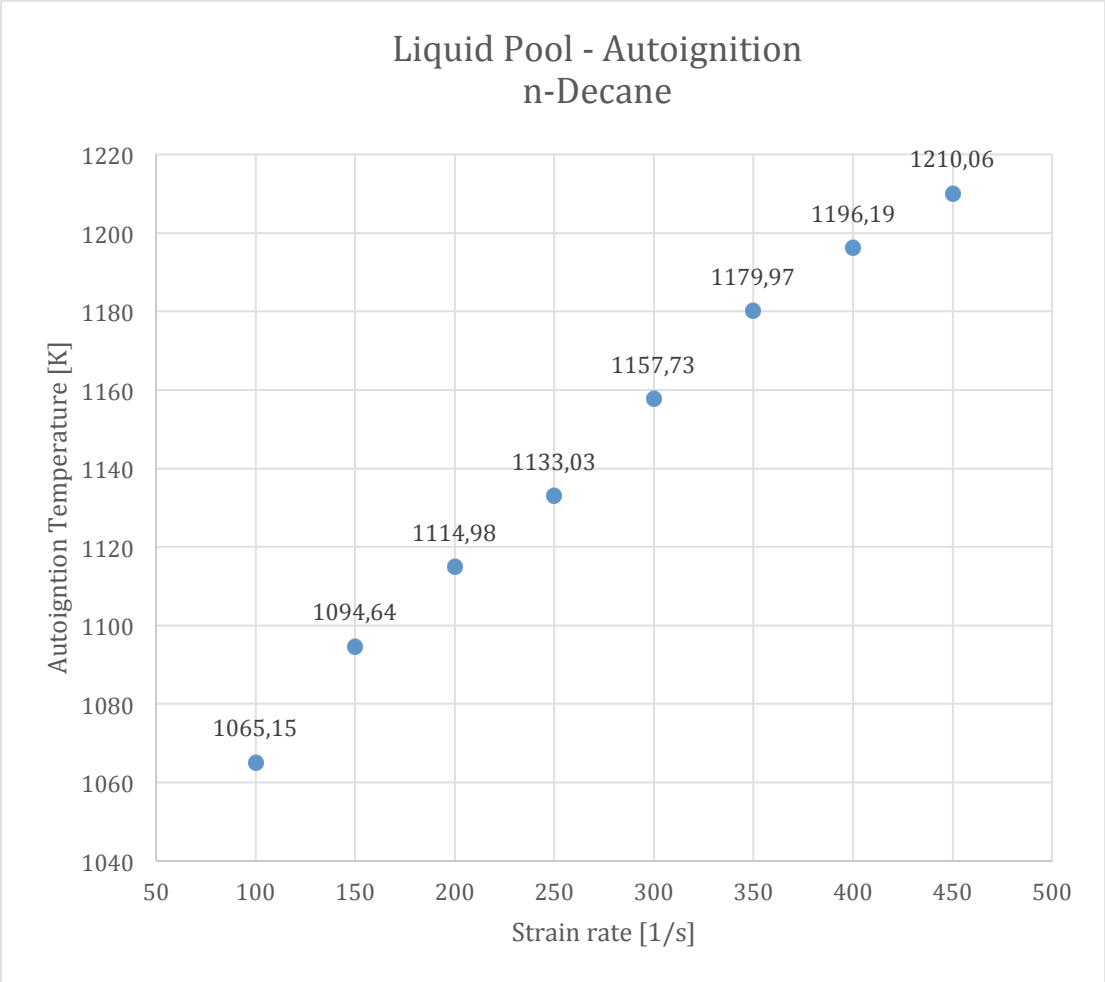

Figure 23: The temperature of the oxidizer stream at autoignition $T_{2,ign}$ as a function of the strain rate a_2 for $Y_{O2,2}$ = 0.23, T_1 = 294.15 [K]

Die approbierte gedruckte Originalversion dieser Diplomarbeit ist an der TU Wien Bibliothek verfügbar.
The approved original version of this thesis is available in print at TU Wien Bibliothek.

Figure 24 shows the temperature of the oxidizer stream at autoignition $T_{2,ign}$ as a function of the strain rate a_2 for a 50% to 50% mix between isobutanol and n-decane.

The strain rate is defined as the axial flow, in other words it can be described as the reciprocal of the characteristic flow time.

So the higher the strain rate of the oxidizer stream, the higher the velocity of the oxidizer stream ($Y_{O2,2}$ = 0.23) flowing through the reaction zone where the ignition takes place.

In order to start an ignition it is important that the reactants (the air of the oxidizer stream and the vapor of the liquid fuel) can mix properly and it is also essential that there is enough time for the ignition-reaction to take place. This means that a high strain rate, respectively a high velocity of the oxidizer stream through the reaction zone can lead to conditions where it is harder to ignite a flame. In other words a higher strain rate can lead to a higher autoignition temperature.

The results in figure 24 show these characteristics pretty well. As expected the autoignition temperature increases with an increasing strain rate.

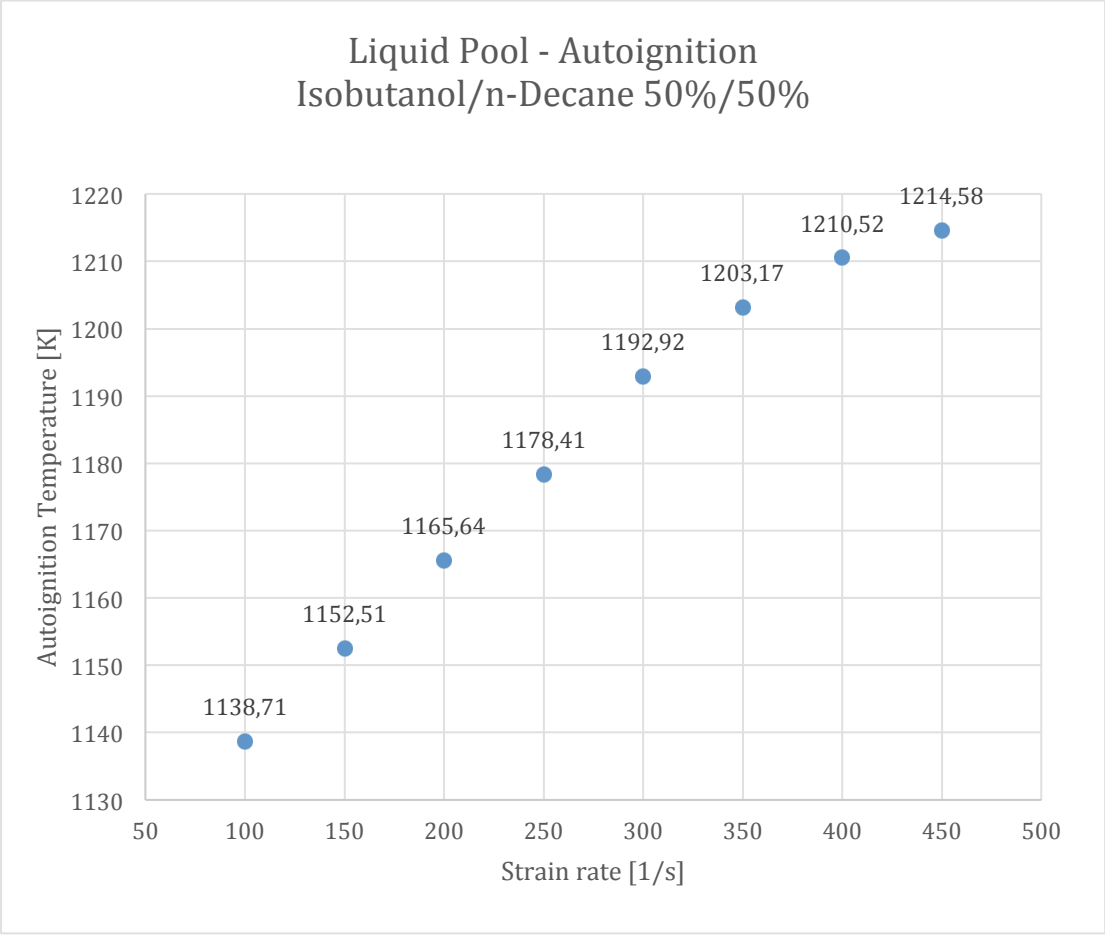

Figure 24: The temperature of the oxidizer stream at autoignition $T_{2,ign}$ as a function of the strain rate a_2 for $Y_{O2,2}$ = 0.23, T_1 = 294.15 [K]

Die approbierte gedruckte Originalversion dieser Diplomarbeit ist an der TU Wien Bibliothek verfügbar.
The approved original version of this thesis is available in print at TU Wien Bibliothek.
TU Bibliothek Your knowledge hub WIEN

Figure 25 shows the temperature of the oxidizer stream at autoignition $T_{2,ign}$ as a function of the strain rate a_2 for n-heptane, n-decane and isobutanol. The figure depicts a comparison between these three fuels and shows that isobutanol has the highest autoignition temperature at a strain rate $a_2 = 180\ s^{-1}$ and below. Furthermore decane has the highest autoignition temperature at the strain rate $a_2 = 380\ s^{-1}$ and above.

The figure also shows two intersection points between heptane and isobutanol at the strain rates of $a_2 = 180\ s^{-1}$ and $a_2 = 310\ s^{-1}$.

Another intersection point is depicted in figure 25 at the strain rate of $a_2 = 380\ s^{-1}$ between all of the three fuels tested.

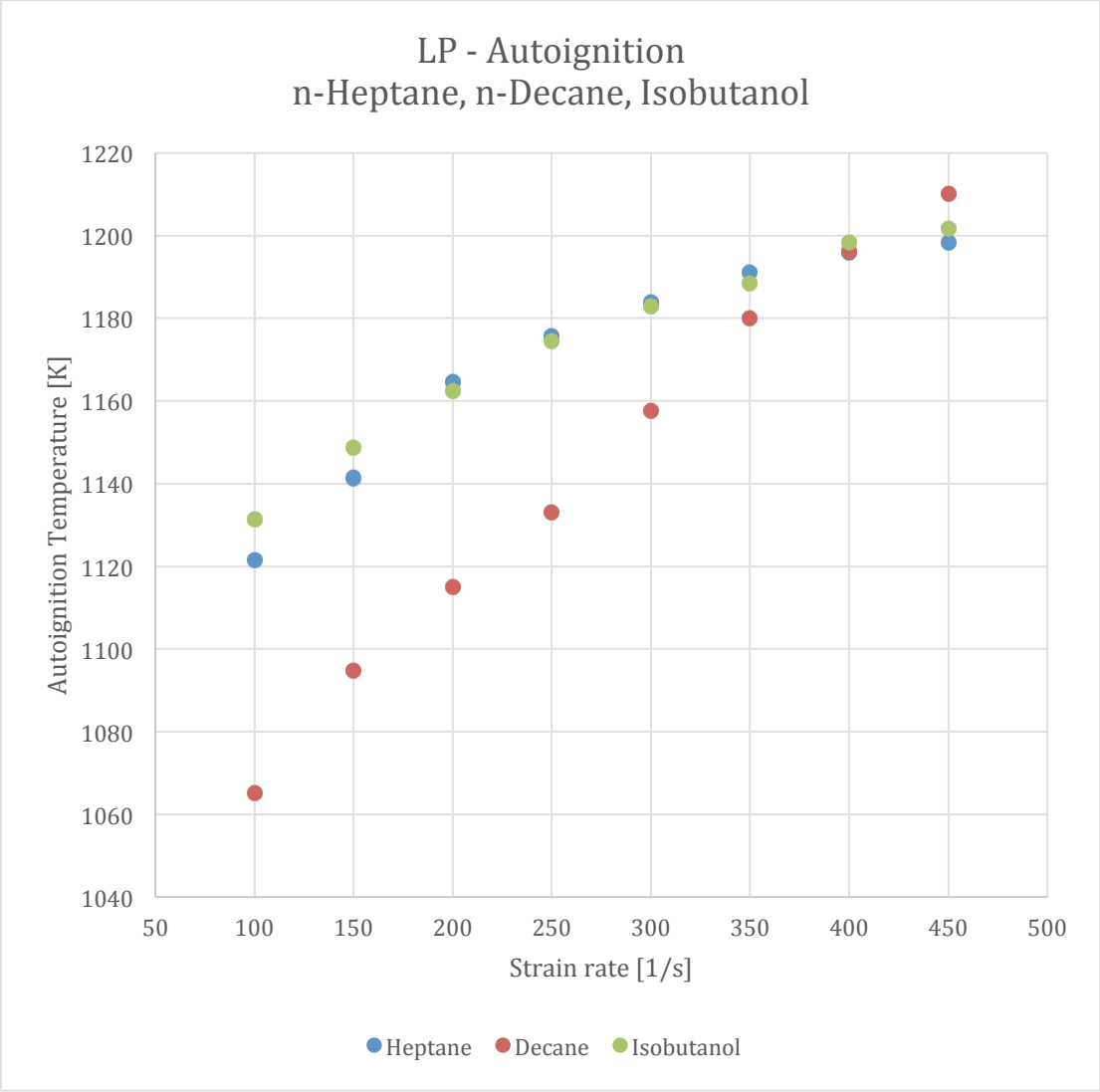

Figure 25: The temperature of the oxidizer stream at autoignition $T_{2,ign}$ as a function of the strain rate a_2 for $Y_{O2,2} = 0.23$, $T_1 = 294.15$ [K]

Die approbierte gedruckte Originalversion dieser Diplomarbeit ist an der TU Wien Bibliothek verfügbar.
The approved original version of this thesis is available in print at TU Wien Bibliothek.

Figure 26 shows the temperature of the oxidizer stream at autoignition $T_{2,ign}$ as a function of the strain rate a_2 for a 50% to 50% mix between isobutanol and n-heptane, pure n-heptane and pure Isobutanol. The figure depicts a comparison between these three fuels and shows that the mix between n-heptane and isobutanol has the highest autoignition temperatures and that there is an intersection point at a strain rate of about a_2 = 200 s^{-1} between n-heptane and isobutanol.

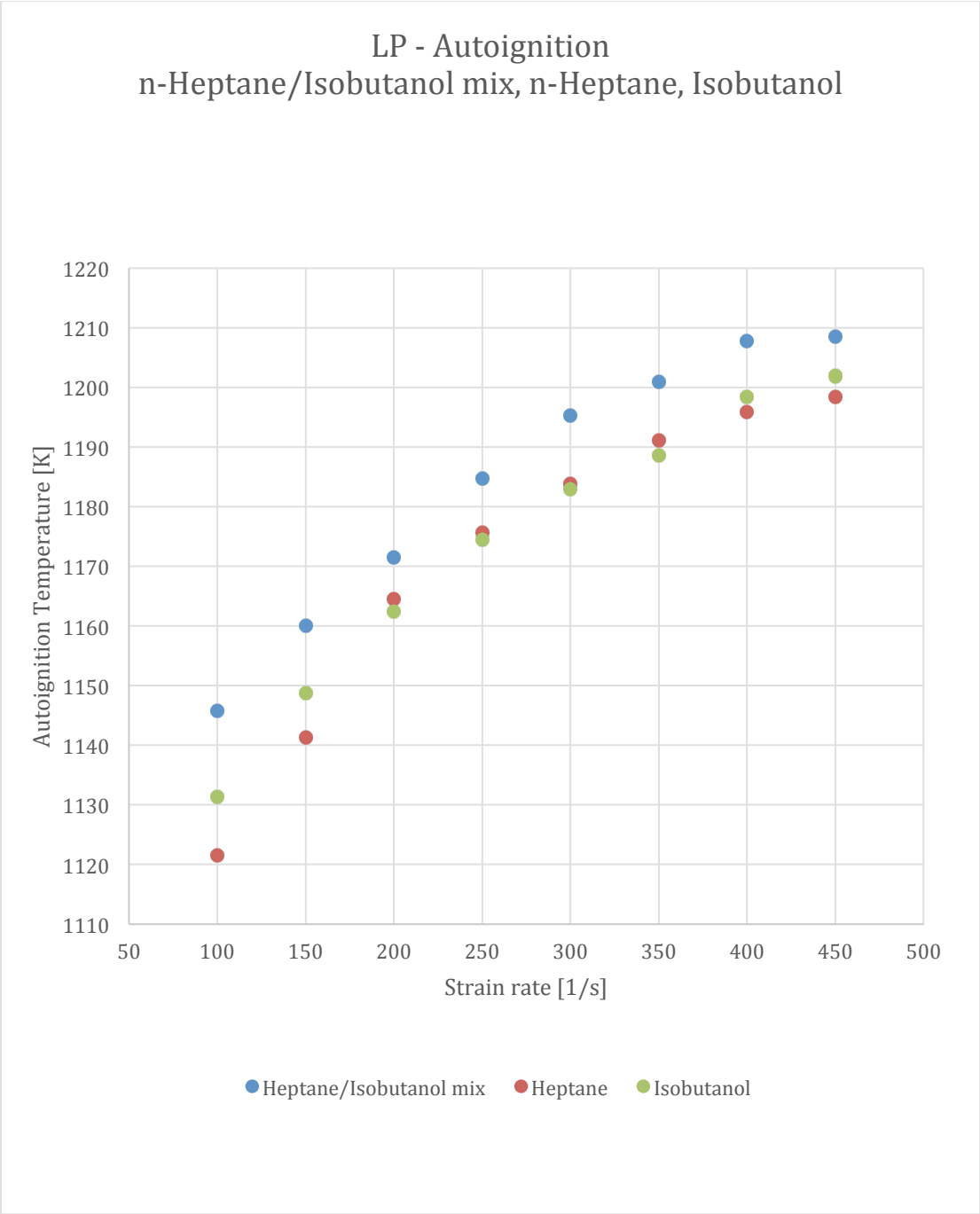

Figure 26: The temperature of the oxidizer stream at autoignition $T_{2,ign}$ as a function of the strain rate a_2 for $Y_{O2,2}$ = 0.23, T_1 = 294.15 [K]

Die approbierte gedruckte Originalversion dieser Diplomarbeit ist an der TU Wien Bibliothek verfügbar.
The approved original version of this thesis is available in print at TU Wien Bibliothek.

Figure 27 shows the temperature of the oxidizer stream at autoignition $T_{2,ign}$ as a function of the strain rate a_2 for a 50% to 50% mix between isobutanol and n-decane, pure n-decane and pure Isobutanol. The figure depicts a comparison between these three fuels and shows that the mix between n-decane and isobutanol has the highest autoignition temperatures and that there is an intersection point at a strain rate of about $a_2 = 400\ s^{-1}$ between n-decane and isobutanol.

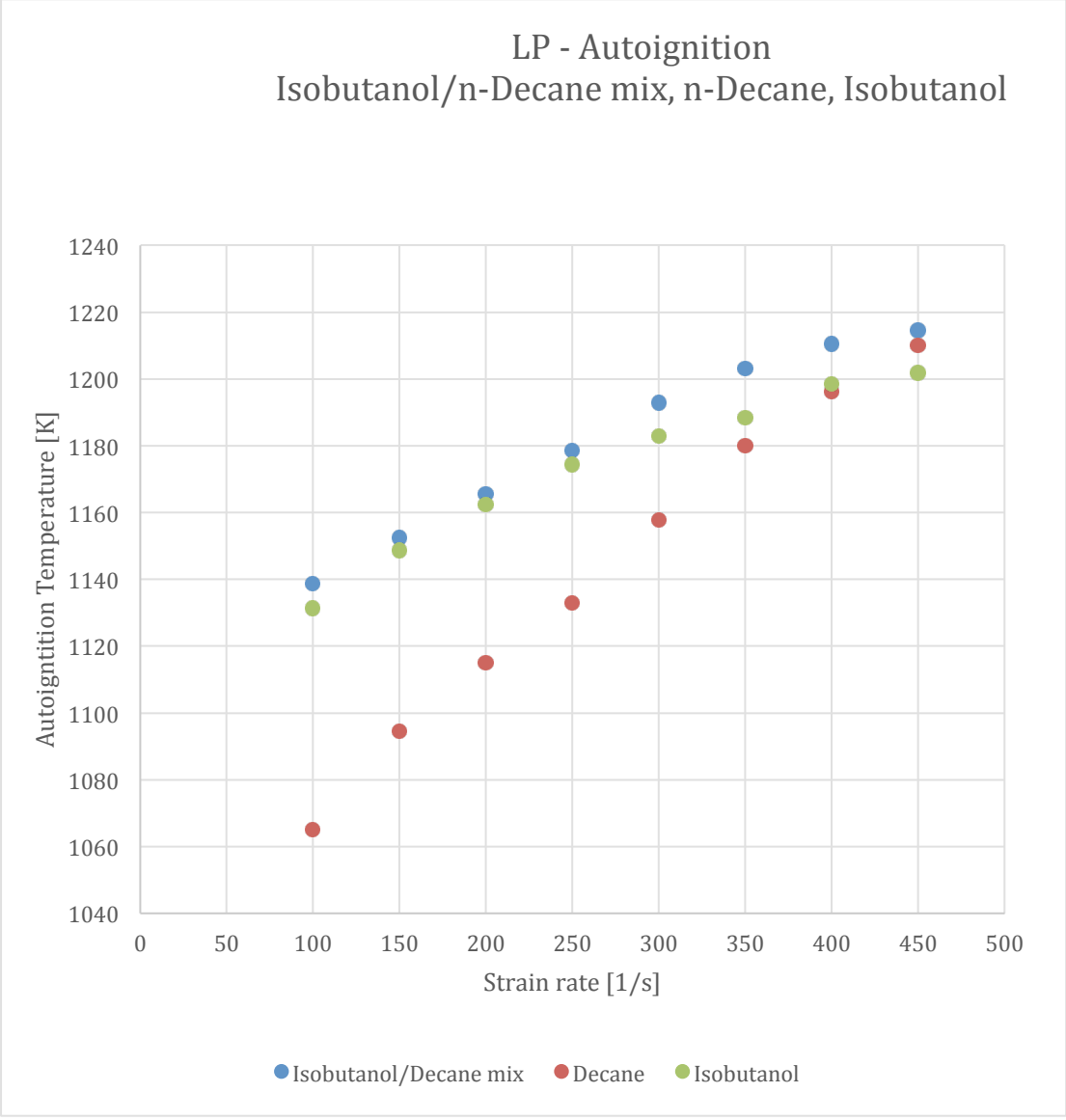

Figure 27: The temperature of the oxidizer stream at autoignition $T_{2,ign}$ as a function of the strain rate a_2 for $Y_{O2,2} = 0.23$, $T_1 = 294.15$ [K]

Die approbierte gedruckte Originalversion dieser Diplomarbeit ist an der TU Wien Bibliothek verfügbar.
The approved original version of this thesis is available in print at TU Wien Bibliothek.

Figure 28 shows the temperature of the oxidizer stream at autoignition $T_{2,ign}$ as a function of the strain rate a_2 for butane.

The strain rate is defined as the axial flow, in other words it can be described as the reciprocal of the characteristic flow time given by the equation

$$a_2 = 2V_2 / L \qquad [32]$$

So the higher the strain rate of the oxidizer stream, the higher the velocity of the oxidizer stream ($Y_{O2,2}$ = 0.23) flowing through the reaction zone where the ignition takes place.

In order to start an ignition it is important that the reactants (the air of the oxidizer stream and the vapor of the liquid fuel) can mix properly and it is also essential that there is enough time for the ignition-reaction to take place. This means that a high strain rate, respectively a high velocity of the oxidizer stream through the reaction zone can lead to conditions where it is harder to ignite a flame. In other words a higher strain rate can lead to a higher autoignition temperature.

The results in figure 28 show these characteristics pretty well. As expected the autoignition temperature increases with an increasing strain rate.

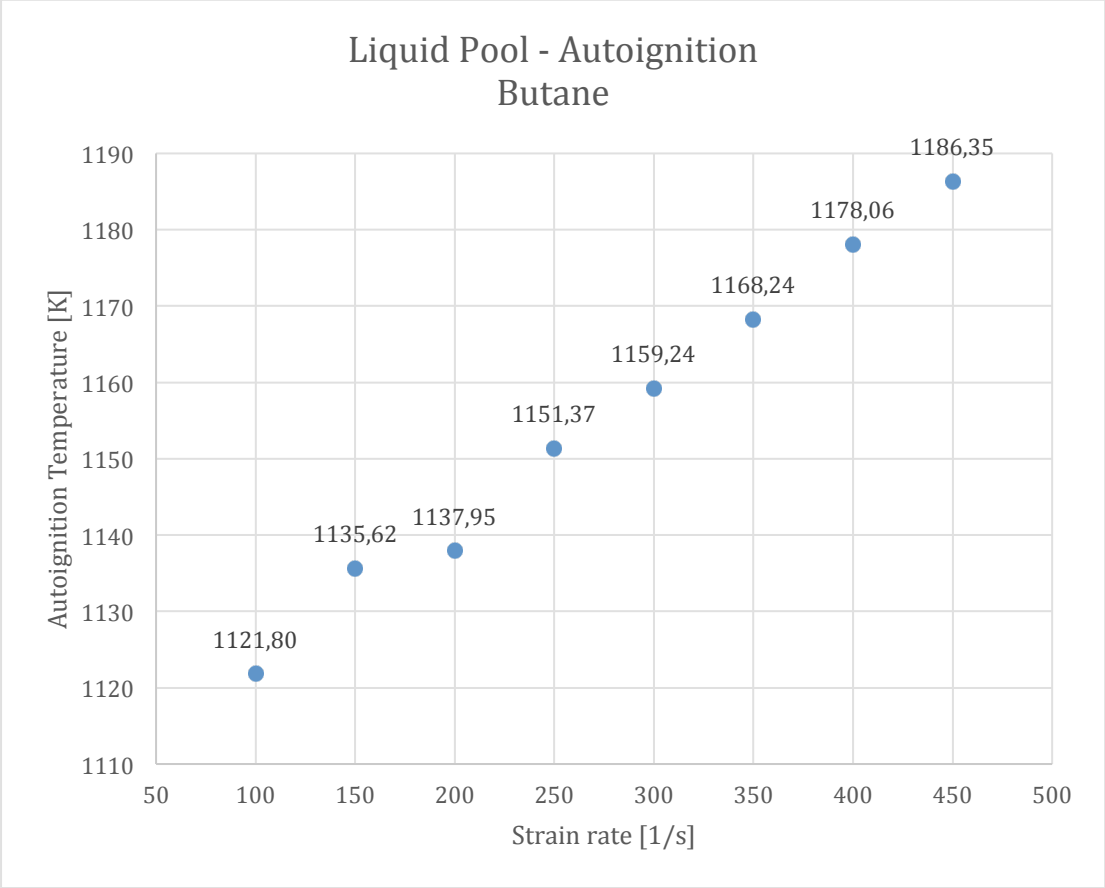

Figure 28: The temperature of the oxidizer stream at autoignition $T_{2,ign}$ as a function of the strain rate a_2 for $Y_{O2,2}$ = 0.23, T_1 = 294.15 [K]

Die approbierte gedruckte Originalversion dieser Diplomarbeit ist an der TU Wien Bibliothek verfügbar.
The approved original version of this thesis is available in print at TU Wien Bibliothek.
TU Bibliothek Your knowledge hub WIEN

5. Concluding remarks

The main focus of this diploma thesis was aimed to help to understand the influence of reactants on critical conditions of autoignition and extinction of propane with the gaseous counterflow burner and n-heptane, isobutanol, n-heptane/isobutanol-mix, 1-propanol, ethanol, n-decane, n- decane/isobutanol-mix and butane with the counterflow liquid pool burner in nonpremixed, nonuniform flows.

Two different configuration setups were employed to carry out experimental studies in order to characterize the critical conditions of the autoignition and extinction events of one hydrocarbon (propane), four alcohols (isobutanol, 1-propanol, ethanol and butane) and two alcohol mixes (n-heptane/isobutanol-mix and n-decane/isobutanol-mix). The first configuration setup is the gaseous counterflow setup and the second configuration is the liquid pool counterflow setup. Both of them can be exchanged with a toggle switch as requested.

For the experiments with the gaseous counterflow burner, propane diluted with nitrogen and an oxidizer stream consisting of pure air was used to measure the critical conditions of autoignition at atmospheric pressure (1.013 bar). The temperature of the oxidizer stream at autoignition as a function of the fuel mass fraction $Y_{F,1}$ at fixed values of $Y_{O2,2}$ = 0.233, and strain rate a_2 = 400 s^{-1} were investigated, as well as the temperature of the oxidizer stream at autoignition as a function of the mass fraction of oxygen $Y_{O2,2}$ at fixed values of $Y_{F,1}$ = 0.21, and strain rate a_2 = 400 s^{-1}.

The critical conditions of autoignition with the liquid pool counterflow burner at atmospheric pressure (1.013 bar) were measured with n-heptane, isobutanol, n-heptane/isobutanol-mix, 1-propanol, ethanol, n-decane, n-decane/isobutanol-mix and butane and an oxidizer stream consisting of oxygen and nitrogen. The temperature of the oxidizer stream at autoignition as a function of the strain rate a_2 at fixed values of $Y_{O2,2}$ = 0.233 were investigated.

The experimental studies of the critical conditions of autoignition for propane show that the autoignition temperature increases with reducing the oxygen mass fraction. The results also show that a variation of the fuel mass fraction has a similar influence on the autoignition temperature compared to a variation of the oxygen mass fraction, so they show the same characteristics.

During the extinction experiments with propane it was found that the extinction strain rate increases almost linear with increasing the fuel mass fraction. The measurement of the critical conditions of extinction were taking place at an ambient pressure level of 1.013 bar with a liquid fuel and with fixed values of $Y_{O2,2}$ = 0.233 and various values of $Y_{F,1}$.

Die approbierte gedruckte Originalversion dieser Diplomarbeit ist an der TU Wien Bibliothek verfügbar.
The approved original version of this thesis is available in print at TU Wien Bibliothek.
TU Bibliothek Your knowledge hub WIEN

The autoignition experiments with the counterflow liquid pool burner for the alcohols and the alcohol-blends show that the autoignition temperature increases with an increasing strain rate. By comparing the different alcohols it came apparent that the characteristics of all the alcohol fuels tested are similar but the overall autoignition temperature level and the rate of their increase per strain rate is different for every fuel tested. These attributes lead to intersection points on certain strain rate levels when the alcohols and the alcohol-blends are being compared to each other.

Die approbierte gedruckte Originalversion dieser Diplomarbeit ist an der TU Wien Bibliothek verfügbar.
The approved original version of this thesis is available in print at TU Wien Bibliothek.
TU Bibliothek Your knowledge hub WIEN

References

[1] Forman A. Williams, Combustion Theory, Second Edition, CRC Press, ISBN: 9780201407778

[2] M. W. Zemansky, Heat and Thermodynamics, New York: McGraw-Hill, 1957.

[3] E. A. Guggenheim, Thermodynamics, New York: Interscience, 1957.

[4] L. D. Landau and E. M. Lifshitz, Statistical Physics, Reading, Mass.: Addison-Wesley, 1969

[5] D. R. Stull and H. Prophet, JANAF Thermochemical Tables, 2nd ed., Washington: National Bureau of Standards, NSRDS-NBS 37 (June 1971)

[6] Journal of Physical and Chemical Reference Data 1, (1972)-present.

[7] Dagaut P, Cathonnet M. J Chem Phys 1990;87:221.

[8] Frenklach M, Wang H, Rabinovitz MJ. Prog Energy Combust Sci 1992;18:47

[9] Hunter JB, Wang H, Litzinger TA, Frenklach M. Combust Flame 1994;97:201.

[10] Dagaut P, Cathonnet M, Boettner JC. Int J Chem Kinet 1991;23:437.

[11] Dagaut P, Cathonnet M, Boettner JC, Guillard F. Combust Sci Technol 1986;56:232.

[12] Cathonnet M. Combust Sci Technol 1994;98:265.

[13] Fristrom RM, Westenberg AA. Flame structure. New York: McGraw-Hill; 1965. Chapter 14.

[14] Irvin Glassman, Richard A. Yetter, Nick G. Glumac, Combustion, Fifth Edition, ELSEVIER, ISBN: 978-0-12-407913-7.

[15] Norton TS, Dryer FL. Combust Sci Technol 1989;63:107.

[16] Colket III MB, Naegeli DW, Glassman I. Proc Combust Inst 1977;16:1023.

[17] Norbert Peters, Combustion Theory, CEFRC Summer School, Princeton, RWTH AACHEN University, July 2010.

[18] J. Warnatz, U. Maas and R. W. Dibble, Combustion - Physical and Chemical Fundamentals, Modeling and Simulation, Experiments, Pollutant Formation, Berlin Heidelberg: Springer, ISBN: 978-3-540-25992-3, 2006.

[19] A. Linan, The asymptotic structure of counterflow diffusion flames for large activation energies, Acta Astronautica, 1(7-8):1007–1039, 1974.

[20] F. E. Fendell, Ignition and extinction in combustion of initially unmixed reactants, Journal of Fluid Mechanics, 21(2):291–303, 1965.

[21] R. Gehmlich, Experimental Studies on Nonpremixed Combustion at Atmospheric and Elevated Pressures, Dissertation, University of California, San Diego, 2015.

[22] G. P. Merker and C. Schwarz, Combustion Engines Development - Mixture Formation, Combustion, Emissions and Simulation, Berlin: Springer, ISBN: 978-3-

Die approbierte gedruckte Originalversion dieser Diplomarbeit ist an der TU Wien Bibliothek verfügbar.
The approved original version of this thesis is available in print at TU Wien Bibliothek.

642-02951-6, 2012.

[23] "NIST Chemistry WebBook, SRD 69," 2018. [Online]. Available: https://webbook.nist.gov/cgi/cbook.cgi?Name=propane&Units=SI. [Accessed 17 07 2019].

[24] "NIST Chemistry WebBook, SRD 69," 2018. [Online]. Available: https://webbook.nist.gov/cgi/cbook.cgi?Name=isobutanol&Units=SI. [Accessed 17 07 2019].

[25] "NIST Chemistry WebBook, SRD 69," 2018. [Online]. Available: https://webbook.nist.gov/cgi/cbook.cgi?Name=propanol&Units=SI. [Accessed 17 07 2019].

[26] "NIST Chemistry WebBook, SRD 69," 2018. [Online]. Available: https://webbook.nist.gov/cgi/cbook.cgi?Name=ethanol&Units=SI. [Accessed 17 07 2019].

[27] "NIST Chemistry WebBook, SRD 69," 2018. [Online]. Available: https://webbook.nist.gov/cgi/cbook.cgi?Name=butane&Units=SI. [Accessed 17 07 2019].

[28] C. R. Shaddix, "Correcting Thermocouple Measurements for Radiation Loss - a critical Review," in *Proceedings of the 33rd National Heat Transfer Conference*, Livermore, 1999.

[29] I. L. Roberts, J. E. Coney and B. M. Gibbs, "sciencedirect," 12 March 2012. [Online]. Available: https://ac.els-cdn.com/S1359431111001529/1-s2.0-S1359431111001529-main.pdf?_tid=9aec1925-1237-44f3-8e9a-63453d177daf&acdnat=1524529470_b746e9b20c24c0167b73589deab7d131. [Accessed 23 April 2018].

[30] "Neutrium," 24 August 2012. [Online]. Available: https://neutrium.net/properties/properties-of-air/. [Accessed 17 July 2019].

[31] "Thermopedia," 2011 February 2011. [Online]. Available: http://www.thermopedia.com/fr/content/553/. [Accessed 17 July 2019].

[32] K. Seshadri, S. Humer, R. Seiser, Activation-energy asymptotic theory of autoignition of condensed hydrocarbon fuels in non-premixed flows with comparison to experiment, Combustion Theory and Modelling, ISSN: 1364-7830

Die approbierte gedruckte Originalversion dieser Diplomarbeit ist an der TU Wien Bibliothek verfügbar.
The approved original version of this thesis is available in print at TU Wien Bibliothek.

Figures

Figure 1: A schematic illustration oft he experimental configuration for counterflow flames for gaseous and liquid fuels

Figure 2: The S-shaped curve showing the maximum temperature in a diffusion flame as a function of the inverse of the scalar dissipation rate at stoichiometric mixture

Figure 3: Temperature and fuel mass fraction profiles over mixture fraction for diffusion flamelet

Figure 4: Schematic illustration of the experimental setup, consisting of the counterflowburner, gas and fuel supply and the mass flow controllers

Figure 5: Schematic section view and image of the burner

Figure 6: InconelTM 600 gauze 200 screen woven from 0.05 mm diameter wire and an ATI 625™ nickel-based alloy stainless steel ring

Figure 7: Schematic section view and image of the extinction top

Figure 8: Schematic section view and image of the autoignition top

Figure 9: Schematic section view and image of the liquid pool burner

Figure 10: Basic control front panel of the counterflow software

Figure 11: Front panel of the calibration VI during the calibration procedure where the deviation of the mass flow controllers is less than $\pm\mathbf{1}\%$ and the standard deviation is less than $\pm\mathbf{0.01}\%$.

Figure 12: High speed image of an autoignition event with propane with a fuel mass fraction of $Y_{F,1}$ 0.21, oxidizer strain rate a_2 = 400 s^{-1} and pure ais as an oxidizer

Figure 13: High speed image of an extinction event with propane with a fuel mass fraction of $Y_{F,1}$ = 0.6, oxidizer strain rate a2 = 366 s^{-1} and pure air as an oxidizer

Figure 14: High speed image of an autoignition event with heptane with an oxidizer strain rate a_2 = 150 s^{-1} and pure air as an oxidizer

Figure 15: The temperature of the oxidizer stream at autoignition, $T_{2,ign}$ as a function of the mass fraction of oxygen $Y_{O2,2}$ for $Y_{F,1}$ = 0.21, T_1 = 294.15 [K] and a_2 = 400 s^{-1}

Figure 16: The temperature of the oxidizer stream at autoignition, $T_{2,ign}$ as a function of the mass fraction of fuel $Y_{F,1}$ for $Y_{O2,2}$ = 0.23, T1 = 294.15 [K] and a_2 = 400 s^{-1}

Figure 17: The extinction strain rate a_2 as a funtion of the oxygen mass fraction $Y_{O2,2}$ for T = 294.15 [K].

Die approbierte gedruckte Originalversion dieser Diplomarbeit ist an der TU Wien Bibliothek verfügbar.
The approved original version of this thesis is available in print at TU Wien Bibliothek.

Figure 18: The temperature of the oxidizer stream at autoignition, $T_{2,ign}$ as a function of the strain rate a_2 for $Y_{O2,2}$ = 0.23, T_1 = 294.15 [K]
Figure 19: The temperature of the oxidizer stream at autoignition, $T_{2,ign}$ as a function of the strain rate a_2 for $Y_{O2,2}$ = 0.23, T_1 = 294.15 [K]
Figure 20: The temperature of the oxidizer stream at autoignition, $T_{2,ign}$ as a function of the strain rate a_2 for $Y_{O2,2}$ = 0.23, T_1 = 294.15 [K]
Figure 21: The temperature of the oxidizer stream at autoignition, $T_{2,ign}$ as a function of the strain rate a_2 for $Y_{O2,2}$ = 0.23, T_1 = 294.15 [K]
Figure 22: The temperature of the oxidizer stream at autoignition, $T_{2,ign}$ as a function of the strain rate a_2 for $Y_{O2,2}$ = 0.23, T_1 = 294.15 [K]
Figure 23: The temperature of the oxidizer stream at autoignition, $T_{2,ign}$ as a function of the strain rate a_2 for $Y_{O2,2}$ = 0.23, T_1 = 294.15 [K]
Figure 24: The temperature of the oxidizer stream at autoignition, $T_{2,ign}$ as a function of the strain rate a_2 for $Y_{O2,2}$ = 0.23, T_1 = 294.15 [K]
Figure 25: The temperature of the oxidizer stream at autoignition, $T_{2,ign}$ as a function of the strain rate a_2 for $Y_{O2,2}$ = 0.23, T_1 = 294.15 [K]
Figure 26: The temperature of the oxidizer stream at autoignition, $T_{2,ign}$ as a function of the strain rate a_2 for $Y_{O2,2}$ = 0.23, T_1 = 294.15 [K]
Figure 27: The temperature of the oxidizer stream at autoignition, $T_{2,ign}$ as a function of the strain rate a_2 for $Y_{O2,2}$ = 0.23, T_1 = 294.15 [K]
Figure 28: The temperature of the oxidizer stream at autoignition, $T_{2,ign}$ as a function of the strain rate a_2 for $Y_{O2,2}$ = 0.23, T_1 = 294.15 [K]

Die approbierte gedruckte Originalversion dieser Diplomarbeit ist an der TU Wien Bibliothek verfügbar.
The approved original version of this thesis is available in print at TU Wien Bibliothek.

APPENDIX

Autoignition – Gaseous counterflow burner

- propane

Δ [K]	$Y_{O2,2}$	$Y_{F,1}$	a2 [1/s]	Oxidizer Stream Velocity [m/s]	Fuel Stream Velocity [m/s]	$T_{2,ign}$ [K]	$T_{2,ign}$ [K] with radiation loss	T_1 [K]	P [Pa]
45,56	0,233	0,21	400	1,2	0,59547	1146,14	1191,70	294,15	1,013
46,58	0,19	0,21	400	1,2	0,59197	1152,47	1199,05	294,15	1,013
47,39	0,15	0,21	400	1,2	0,58899	1157,41	1204,80	294,15	1,013
48,13	0,11	0,21	400	1,2	0,58617	1161,87	1210,00	294,15	1,013
49,91	0,07	0,21	400	1,2	0,58184	1172,45	1222,36	294,15	1,013
Δ [K]	$Y_{F,1}$	$Y_{O2,2}$	a2 [1/s]	Oxidizer Stream Velocity [m/s]	Fuel Stream Velocity [m/s]	$T_{2,ign}$ [K]	$T_{2,ign}$ [K] with radiation loss	T_1 [K]	P [Pa]
44,24	0,3	0,23	400	1,2	0,58694	1137,76	1182,00	294,15	1,013
43,37	0,35	0,23	400	1,2	0,58234	1132,13	1175,50	294,15	1,013
43,20	0,4	0,23	400	1,2	0,57649	1131,06	1174,26	294,15	1,013
42,70	0,45	0,23	400	1,2	0,57114	1127,77	1170,47	294,15	1,013
42,35	0,5	0,23	400	1,2	0,56544	1125,5	1167,85	294,15	1,013
41,94	0,55	0,23	400	1,2	0,55978	1122,74	1164,68	294,15	1,013
41,84	0,6	0,23	400	1,2	0,55353	1122,07	1163,91	294,15	1,013

TU Bibliothek Your knowledge hub WIEN
Die approbierte gedruckte Originalversion dieser Diplomarbeit ist an der TU Wien Bibliothek verfügbar.
The approved original version of this thesis is available in print at TU Wien Bibliothek.

Die approbierte gedruckte Originalversion dieser Diplomarbeit ist an der TU Wien Bibliothek verfügbar.
The approved original version of this thesis is available in print at TU Wien Bibliothek.

- propane

$Y_{O2,2}$	$Y_{F,1}$	a2 [1/s]	Oxidizer Stream Velocity [m/s]	Fuel Stream Velocity [m/s]	T_1 [K]	P [Pa]
0,233	0,6	604	1,51	1,36	295,15	1,013
0,23	0,6	537	1,3425	1,21	295,15	1,013
0,225	0,6	491	1,2275	1,10	295,15	1,013
0,22	0,6	466	1,165	1,05	295,15	1,013
0,215	0,6	415	1,0375	0,93	295,15	1,013
0,21	0,6	366	0,92	0,82	295,15	1,013
0,205	0,6	319	0,80	0,72	295,15	1,013
0,2	0,6	266	0,67	0,60	295,15	1,013
0,195	0,6	235	0,59	0,53	295,15	1,013

Die approbierte gedruckte Originalversion dieser Diplomarbeit ist an der TU Wien Bibliothek verfügbar.
The approved original version of this thesis is available in print at TU Wien Bibliothek.

• n-heptane

Δ [K]	a2 [1/s]	$Y_{O2,2}$	Oxidizer Stream Velocity [m/s]	$T_{2,ign}$ [K]	$T_{2,ign}$ [K] with radiation loss	T_1 [K]	P [Pa]
51,56	100	0,23	0,3	1069,88	1121,44	294,15	1,013
50,12	150	0,23	0,45	1091,23	1141,35	294,15	1,013
50,25	200	0,23	0,6	1114,25	1164,50	294,15	1,013
49,16	250	0,23	0,75	1126,44	1175,60	294,15	1,013
48,07	300	0,23	0,9	1135,71	1183,78	294,15	1,013
47,17	350	0,23	1,05	1143,96	1191,13	294,15	1,013
46,15	400	0,23	1,2	1149,78	1195,93	294,15	1,013
45,00	450	0,23	1,35	1153,43	1198,43	294,15	1,013

• Isobutanol

Δ [K]	a2 [1/s]	$Y_{O2,2}$	Oxidizer Stream Velocity [m/s]	$T_{2,ign}$ [K]	$T_{2,ign}$ [K] with radiation loss	T_1 [K]	P [Pa]
53,19	100	0,23	0,3	1078,16	1131,35	294,15	1,013
51,27	150	0,23	0,45	1097,38	1148,65	294,15	1,013
49,94	200	0,23	0,6	1112,54	1162,48	294,15	1,013
48,99	250	0,23	0,75	1125,47	1174,46	294,15	1,013
47,96	300	0,23	0,9	1135,04	1183,00	294,15	1,013
46,81	350	0,23	1,05	1141,76	1188,57	294,15	1,013
46,50	400	0,23	1,2	1151,94	1198,44	294,15	1,013
45,47	450	0,23	1,35	1156,41	1201,88	294,15	1,013

Die approbierte gedruckte Originalversion dieser Diplomarbeit ist an der TU Wien Bibliothek verfügbar.
The approved original version of this thesis is available in print at TU Wien Bibliothek.

- isobutanol/n-heptane – mix

Δ [K]	a2 [1/s]	$Y_{O2,2}$	Oxidizer Stream Velocity [m/s]	$T_{2,ign}$ [K]	$T_{2,ign}$ [K] with radiation loss	T_1 [K]	P [Pa]
55,61	100	0,23	0,3	1090,17	1145,78	294,15	1,013
53,11	150	0,23	0,45	1107,05	1160,16	294,15	1,013
51,34	200	0,23	0,6	1120,19	1171,53	294,15	1,013
50,53	250	0,23	0,75	1134,18	1184,71	294,15	1,013
49,75	300	0,23	0,9	1145,47	1195,22	294,15	1,013
48,57	350	0,23	1,05	1152,33	1200,90	294,15	1,013
47,80	400	0,23	1,2	1159,89	1207,69	294,15	1,013
46,37	450	0,23	1,35	1162,1	1208,47	294,15	1,013

- propanol

Δ [K]	a2 [1/s]	$Y_{O2,2}$	Oxidizer Stream Velocity [m/s]	$T_{2,ign}$ [K]	$T_{2,ign}$ [K] with radiation loss	T_1 [K]	P [Pa]
49,81	100	0,23	0,3	1060,75	1110,56	294,15	1,013
47,62	150	0,23	0,45	1077,41	1125,03	294,15	1,013
46,98	200	0,23	0,6	1095,72	1142,70	294,15	1,013
46,92	250	0,23	0,75	1113,43	1160,35	294,15	1,013
47,61	300	0,23	0,9	1133,02	1180,63	294,15	1,013
47,43	350	0,23	1,05	1145,53	1192,96	294,15	1,013
47,29	400	0,23	1,2	1156,83	1204,12	294,15	1,013
46,69	450	0,23	1,35	1164,06	1210,75	294,15	1,013

Die approbierte gedruckte Originalversion dieser Diplomarbeit ist an der TU Wien Bibliothek verfügbar.
The approved original version of this thesis is available in print at TU Wien Bibliothek.

• ethanol

Δ [K]	a2 [1/s]	$Y_{O2,2}$	Oxidizer Stream Velocity [m/s]	$T_{2,ign}$ [K]	$T_{2,ign}$ [K] with radiation loss	T_1 [K]	P [Pa]
49,82	100	0,23	0,3	1060,77	1110,59	294,15	1,013
48,15	150	0,23	0,45	1080,43	1128,58	294,15	1,013
47,57	200	0,23	0,6	1099,13	1146,70	294,15	1,013
47,85	250	0,23	0,75	1118,88	1166,73	294,15	1,013
47,91	300	0,23	0,9	1134,76	1182,67	294,15	1,013
47,70	350	0,23	1,05	1147,13	1194,83	294,15	1,013
47,13	400	0,23	1,2	1155,86	1202,99	294,15	1,013
46,93	450	0,23	1,35	1165,57	1212,50	294,15	1,013

• n-decane

Δ [K]	a2 [1/s]	$Y_{O2,2}$	Oxidizer Stream Velocity [m/s]	$T_{2,ign}$ [K]	$T_{2,ign}$ [K] with radiation loss	T_1 [K]	P [Pa]
42,92	100	0,23	0,3	1022,23	1065,15	294,15	1,013
43,17	150	0,23	0,45	1051,47	1094,64	294,15	1,013
43,01	200	0,23	0,6	1071,97	1114,98	294,15	1,013
43,07	250	0,23	0,75	1089,96	1133,03	294,15	1,013
44,38	300	0,23	0,9	1113,35	1157,73	294,15	1,013
45,60	350	0,23	1,05	1134,37	1179,97	294,15	1,013
46,18	400	0,23	1,2	1150,01	1196,19	294,15	1,013
46,59	450	0,23	1,35	1163,47	1210,06	294,15	1,013

Die approbierte gedruckte Originalversion dieser Diplomarbeit ist an der TU Wien Bibliothek verfügbar.
The approved original version of this thesis is available in print at TU Wien Bibliothek.

- isobutanol/n-decane – mix

Δ [K]	a2 [1/s]	$Y_{O2,2}$	Oxidizer Stream Velocity [m/s]	$T_{2,ign}$ [K]	$T_{2,ign}$ [K] with radiation loss	T_1 [K]	P [Pa]
54,41	100	0,23	0,3	1084,30	1138,71	294,15	1,013
51,88	150	0,23	0,45	1100,63	1152,51	294,15	1,013
50,43	200	0,23	0,6	1115,21	1165,64	294,15	1,013
49,58	250	0,23	0,75	1128,83	1178,41	294,15	1,013
49,41	300	0,23	0,9	1143,51	1192,92	294,15	1,013
48,90	350	0,23	1,05	1154,27	1203,17	294,15	1,013
48,20	400	0,23	1,2	1162,32	1210,52	294,15	1,013
47,22	450	0,23	1,35	1167,36	1214,58	294,15	1,013

x

- butane

Δ [K]	a2 [1/s]	$Y_{O2,2}$	Oxidizer Stream Velocity [m/s]	$T_{2,ign}$ [K]	$T_{2,ign}$ [K] with radiation loss	T_1 [K]	P [Pa]
51,62	100	0,23	0,3	1070,18	1121,80	294,15	1,013
49,23	150	0,23	0,45	1086,39	1135,62	294,15	1,013
46,28	200	0,23	0,6	1091,67	1137,95	294,15	1,013
45,63	250	0,23	0,75	1105,74	1151,37	294,15	1,013
44,59	300	0,23	0,9	1114,65	1159,24	294,15	1,013
43,99	350	0,23	1,05	1124,25	1168,24	294,15	1,013
43,71	400	0,23	1,2	1134,35	1178,06	294,15	1,013
43,38	450	0,23	1,35	1142,97	1186,35	294,15	1,013